RadioGraphics

MR Imaging of Myocardial Infarction[1]

Prabhakar Rajiah, MD, FRCR • Milind Y. Desai, MD • Deborah Kwon, MD
Scott D. Flamm, MD, MBA

Scan this code for access to supplemental material on our website.

TEACHING POINTS
See last page

Magnetic resonance (MR) imaging plays an important role in evaluation of various aspects of myocardial infarction (MI). MR imaging is useful in establishing the diagnosis of acute MI, particularly in patients who present with symptoms of MI but outside the diagnostic time frame of altered cardiac enzyme levels or with clinical features of acute MI but without an angiographic culprit lesion. MR imaging is valuable in establishing a diagnosis of chronic MI and distinguishing this condition from nonischemic cardiomyopathies, mainly through use of delayed-enhancement patterns. MR imaging also provides clinicians with several prognostic indicators that enable risk stratification, such as scar burden, microvascular obstruction, hemorrhage, and peri-infarct ischemia. The extent and transmurality of scar burden have been shown to have independent and incremental prognostic power over a range of left ventricular function. The extent of scarring at MR imaging is an important predictor of successful outcome after revascularization procedures, and extensive scarring in the lateral wall indicates poor outcome after cardiac resynchronization therapy. Scar size at MR imaging is also a useful surrogate end point in clinical trials. Finally, MR imaging can be used to detect complications of MI, such as aneurysms, pericarditis, ventricular septal defect, thrombus, and mitral regurgitation. Supplemental material available at *http://radiographics.rsna.org/lookup/suppl/doi:10.1148/rg.335125722/-/DC1.*

Abbreviations: ACS = acute coronary syndrome, ECG = electrocardiography, FDG = ^{18}F fluorodeoxyglucose, FSE = fast spin-echo, GRE = gradient-echo, HCM = hypertrophic cardiomyopathy, LAD = left anterior descending coronary artery, LBBB = left bundle-branch block, LCX = left circumflex coronary artery, LV = left ventricle, MI = myocardial infarction, RCA = right coronary artery, RV = right ventricle, SENC = strain encoding, SSFP = steady-state free-precession, STEMI = ST-segment elevation MI, STIR = short-inversion-time inversion-recovery, 3D = three-dimensional, 2D = two-dimensional

RadioGraphics 2013; 33:1383–1412 • **Published online** 10.1148/rg.335125722 • **Content Codes:** CA MR

[1]From the Cardiothoracic Imaging Section, University Hospitals of Cleveland, Case Western Reserve University School of Medicine, Cleveland, Ohio (P.R.); and Cardiovascular Imaging Laboratory, J1-4, Imaging Institute, and Cardiovascular Medicine, Heart and Vascular Institute, Cleveland Clinic, 9500 Euclid Ave, Cleveland, OH 44195 (M.Y.D., D.K., S.D.F.). Received April 4, 2012; revision requested July 18; final revision received January 22, 2013; accepted January 30. D.K. and S.D.F. have disclosed financial relationships (see p 1408); all other authors have no relevant relationships to disclose. **Address correspondence to** S.D.F. (e-mail: *flamms@ccf.org*).

Introduction

Myocardial infarction (MI) is defined as myocardial cell death secondary to prolonged ischemia that results in an inadequate supply of oxygenated blood to an area of the myocardium, particularly when ischemia exceeds a critical threshold that overwhelms cellular repair mechanisms. MI is typically caused by luminal thrombosis superimposed on coronary atherosclerosis; occasionally, it can be caused by coronary spasm, coronary embolism, or thrombosis in nonatherosclerotic vessels. Arteritis, dissection, congenital abnormalities, hypercoagulable states, and cocaine use are uncommon causes.

MI is the leading cause of death and a main cause of morbidity in the United States. Each year, more than 1.2 million people in the United States experience MI. In these patients, MI may present as a major catastrophic event, such as sudden cardiac death, or as a minor event in a chronic disease; MI may also remain silent. Approximately 0.5 million patients who experience MI die before reaching a hospital (1). However, patients who present to the hospital with MI have a survival rate of 90%–95%. MI is most commonly observed in patients aged 40–65 years. Unfortunately, MIs are more typically severe or lethal in women (1).

Magnetic resonance (MR) imaging plays an important role in evaluating the various stages of MI. MR imaging has several advantages over other imaging modalities: it is noninvasive, does not require patients to be exposed to radiation, and has good spatiotemporal resolution, contrast resolution that enables tissue characterization, a wide field of view, and multiplanar reconstruction capabilities. However, MR imaging is contraindicated in patients with particular metallic devices, claustrophobia, or severe renal dysfunction because of the risk of nephrogenic systemic fibrosis.

In this article, we review the uses of MR imaging in assessing MI, including establishing the diagnosis, characterizing the infarct, determining the age of the infarct, stratifying risk, predicting response to therapy, and evaluating complications (Table 1).

Table 1
Roles of MR Imaging in MI

Establishing diagnosis
Acute MI
Angiogram normal, no coronary artery disease: evaluate for other causes (takotsubo cardiomyopathy, myocarditis, etc)
Angiogram normal, recanalization of vessel: identify MI
Multivessel coronary disease on angiogram: identify the infarct-related artery
Establish diagnosis before angiography or elevation of troponin level
Chronic MI
Congestive cardiac failure
Iatrogenic infarct
Establishing age of infarct
Stratifying risk
Acute MI
Reversible versus irreversible injury
Transmurality
Microvascular obstruction
Chronic MI
Scar size
Missed infarcts
Other prognostic indicators
Hemorrhage in core of infarct
Ischemia
Predicting response to therapy
Coronary revascularization
Cardiac resynchronization therapy
Detecting complications
Free-wall rupture
Ventricular septal rupture
Aneurysm or pseudoaneurysm
Pericardial effusion or pericarditis
Thrombus
Mitral regurgitation
Infarction of RV or right atrium
Chronic congestive heart failure
Experimental applications
Use in emergency room
Coronary artery imaging
Evaluation of new therapeutic approaches

Note.—RV = right ventricle.

Myocardial Infarction

In MI, biochemical and functional abnormalities begin immediately after the onset of ischemia; loss of contractility occurs in 60 seconds and loss of viability occurs in 20–40 minutes. The changes progress from the initial decrease in perfusion, leading to diminished tissue oxygenation, decreased phosphocreatine, repolarization abnormalities, diastolic dysfunction, systolic dysfunction, decreased adenosine triphosphate, edema, and finally tissue necrosis. The infarct progresses like a "wavefront" from the endocardium to the epicardium (Fig 1). Complete necrosis takes 2–4 hours or longer, depending on the presence of collateral circulation, persistent or intermittent coronary arterial occlusion, sensitivity of myocytes to ischemia, precondi-

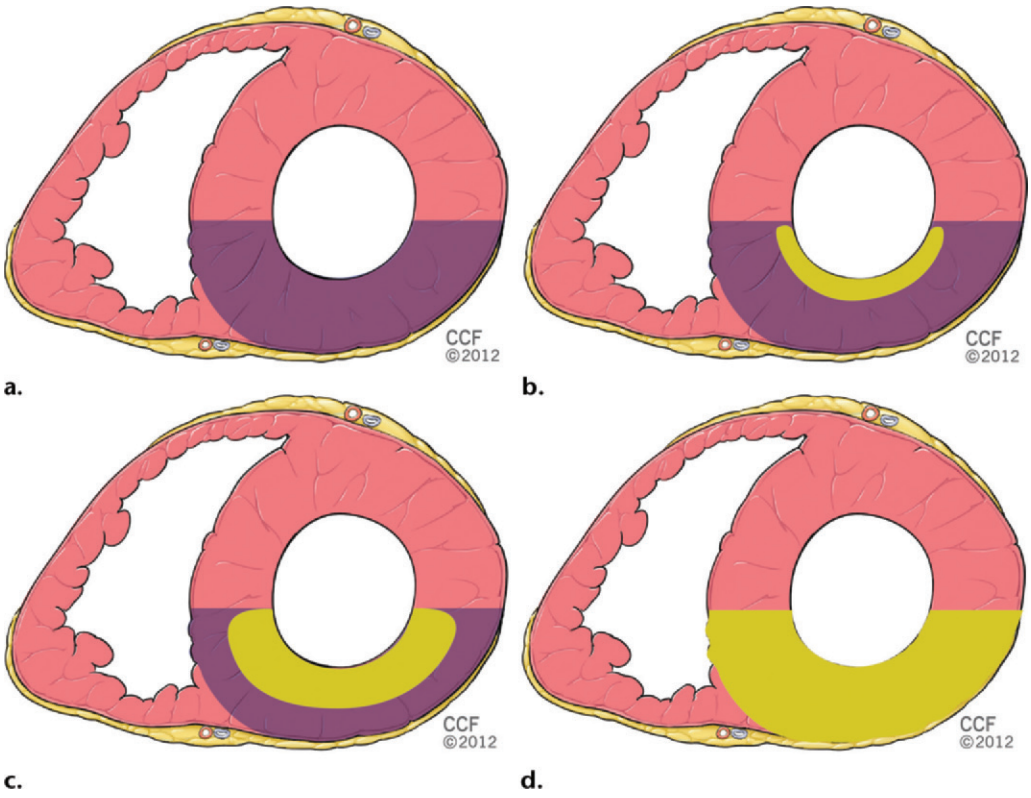

Figure 1. Wavefront phenomenon of myocardial ischemic cell death. Irreversible injury of ischemic myocardium progresses as a wavefront, occurring first in the subendocardial myocardium but ultimately becoming transmural if ischemia persists. Pink = nonischemic, purple = ischemic, yellow = necrotic. **(a)** At 15 minutes, there is ischemic myocardium but no infarct. **(b)** At 40 minutes, subendocardial infarction is seen. **(c)** At 3 hours, the subendocardial infarction is seen extending to the midmyocardial region. **(d)** Beyond 6 hours, the infarct becomes transmural, extending from the subendocardial to the subepicardial layers.

Table 2
Types of MI

Type	Description
1	Spontaneous MI related to plaque erosion or rupture, fissuring, or dissection
2	MI secondary to increased oxygen demand or decreased oxygen supply (coronary artery spasm, coronary embolism, anemia, arrhythmia, hypertension, or hypotension)
3	Sudden unexpected cardiac death with symptoms suggestive of myocardial ischemia, new ST-segment elevation or LBBB, or evidence of fresh thrombus in coronary artery at angiography or autopsy
4a	MI associated with percutaneous coronary intervention
4b	MI associated with stent thrombosis at angiography or autopsy
5	MI associated with coronary artery bypass grafting

Source.—Adapted, with permission, from reference 2. LBBB = left bundle-branch block.

tioning, and individual demand for myocardial oxygen and nutrients.

An infarct is termed microscopic when <10% of the myocardium is involved, moderate when 10%–30% is involved, and large when >30% is involved (2). Transmural MI affects the full thickness of affected muscle segments, from endocardium through midmyocardium to epicardium; nontransmural MI does not extend through the full thickness of the myocardial segments and is limited to endocardium or to endocardium plus midmyocardium. Clinically, MI can occur as either ST-segment elevation MI (STEMI) or non–ST-segment elevation MI (NSTEMI). The various types of MI, as defined by the European Heart Society and American College of Cardiology, are summarized in Table 2 (2).

Table 3
Typical MR Imaging Protocol for Evaluation of MI

Sequences	Imaging Planes	Utility	Acquisition Time
Mandatory sequences			
Scout sequences	Axial, sagittal, coronal	Use as localizer; determine coil position	30 sec
Single-shot SSFP or FSE	Axial stack, breath-hold	Obtain overview; plan for cardiac views	15–30 sec (one breath hold)
Cine SSFP	VLA, HLA, four-chamber long-axis, LVOT long-axis, short-axis stack	Assess morphology, volumes, and function (global, regional)	5–8 min
Delayed enhancement	Look-Locker (TI scout) sequence allows determination of inversion-recovery time; phase-sensitive inversion-recovery: VLA, LVOT long-axis, four-chamber long-axis; 3D contiguous volume short-axis stack	Diagnose MI and infarct size; assess myocardial viability and scar pattern in nonischemic cardiomyopathy; detect thrombus, pericardial enhancement	5 min
Optional sequences			
T2-weighted TSE with or without fat suppression	VLA, four-chamber long-axis, LVOT long-axis, short-axis stack	Assess morphology; detect myocardial edema and pericardial effusion or thickening	3 min
First-pass perfusion	Rest and stress: short-axis, three or four sections	Identify ischemia or infarct; stratify risk after MI	1–2 min each
Cine images after dobutamine infusion	Short-axis	Evaluate contractile reserve as improvement in wall thickening	3–5 min
Velocity-encoded phase-contrast	Ascending aorta, SVC, RSPV flow; velocity encoding through plane = 200 cm/sec	Quantify regurgitation or stenosis; estimate shunt volume	15–25 sec
3D whole-heart navigator-gated coronary angiography	Axial	Evaluate proximal coronary arteries and coronary anomalies	3–8 min
Myocardial tagging	Short-axis, three sections	Quantify regional myocardial function	1–3 min

Note.—FSE = fast spin-echo, HLA = horizontal long-axis, LVOT = left ventricular (LV) outflow tract (paraseptal long-axis or three-chamber long-axis), RSPV = right superior pulmonary vein, SSFP = steady-state free-precession, SVC = superior vena cava, 3D = three-dimensional, TI = inversion time, TSE = turbo spin-echo, VLA = vertical long-axis (two-chamber long-axis).

MR Imaging Protocol

A combination of various MR imaging sequences can be used to evaluate a patient with suspected or established MI; each sequence provides information about a different aspect of the disease. A standardized protocol for evaluation of such patients is listed in Table 3. Sequences can be added or modified depending on the individual clinical scenario and the patient (eg, presence or absence of arrhythmia, breath-holding ability).

A bare-bones MR imaging protocol for evaluation of myocardial viability can be performed in as little as 15–20 minutes. This protocol includes scout images, axial SSFP or FSE images, cine images in multiple long- and short-axis

planes, and delayed-enhancement images. Optional sequences may be added depending on the clinical indication; adding these sequences will increase the imaging time. These optional sequences include stress and rest first-pass perfusion images, cine images after dobutamine infusion, myocardial tagging, 3D whole-heart coronary angiography, phase-contrast images, T2-weighted images, and early postcontrast enhanced images.

Mandatory Sequences

Scout images are used in planning subsequent cardiac views and confirming that the heart is positioned at the center of the coil. Axial single-shot SSFP or FSE images through the chest are used to detect gross abnormalities in the thorax and plan subsequent cardiac views. Cine-SSFP sequences in multiple planes orthogonal to the heart are used in determination of ventricular and valvular function. Ventricular volumes, mass, and ejection fraction can be quantified by drawing endocardial and epicardial contours on end-diastolic and end-systolic images from contiguous datasets spanning the ventricles.

Teaching Point

Delayed-enhancement imaging is the most important technique for evaluation of MI. It is the most accurate method for diagnosing MI or nonischemic cardiomyopathies, quantifying the scar, assessing viability, and evaluating thrombus. Delayed-enhancement imaging typically is performed using a segmented k-space inversion-recovery gradient-echo (GRE) pulse sequence, with the inversion time set to null the signal from normal myocardium. Hyperenhancement is seen as a bright area of tissue against the background of dark normal myocardium.

Delayed-enhancement images can be acquired using two-dimensional (2D), 3D, single-shot, or phase-sensitive inversion-recovery techniques. In the 2D technique, each section is acquired during a single breath hold, with data acquired during every heartbeat or every other heartbeat. In the 3D volumetric technique, the entire LV can be covered in a single breath hold or with free breathing using navigator gating of the diaphragmatic movements, effectively freezing respiratory motion. Single-shot sequences acquire each section within a single heartbeat, which is particularly valuable in patients with arrhythmias or those who have difficulty with breath holds. The phase-sensitive inversion-recovery sequence reduces the need for selecting the optimal inversion time.

With the delayed-enhancement technique, patients undergo imaging 10–20 minutes after administration of gadolinium-chelate (0.1–0.2 mmol/kg body weight; half-life in blood, approximately 20 minutes). The gadolinium-chelate is biologically inert and does not cross intact cell membranes, but passively diffuses within the myocardium in the extracellular interstitial space. In normal myocardium, the myocytes are densely packed, so gadolinium has a low volume of distribution (~15%) and is rapidly washed in and washed out; as a result, there is no abnormal enhancement.

Hyperenhancement occurs when there is absence of viable myocytes (3) and the abnormal tissue has an increased volume of distribution of gadolinium (~70%–85%) and slower wash-in and washout of gadolinium, allowing greater accumulation of gadolinium and therefore increased T1-shortening. In acute myocardial injury such as acute MI or acute myocarditis, the rupture of cell membranes allows increased diffusion of gadolinium inside the myocytes (in previously intact intracellular space), resulting in hyperenhancement (4). Finally, scar tissue associated with MI and interstitial fibrosis associated with other diseases lead to reduction in the intracellular space and expansion of the extracellular space, which creates a higher volume of distribution of gadolinium and slower wash-in and washout, resulting in accumulation of gadolinium and hyperenhancement.

Optional Sequences

First-pass perfusion imaging is not required for detection of MI but is an optional technique that is sensitive and accurate in detection of periinfarct ischemia (5), which is useful for risk stratification after MI. Perfusion imaging typically is performed after pharmacologic stress with either adenosine or dipyridamole and then again at rest approximately 15 minutes after stress imaging to allow blood pool washout of gadolinium-chelate. Intravenous gadolinium produces T1-shortening of normal myocardium, resulting in bright signal on T1-weighted images. Hypoperfused areas (eg,

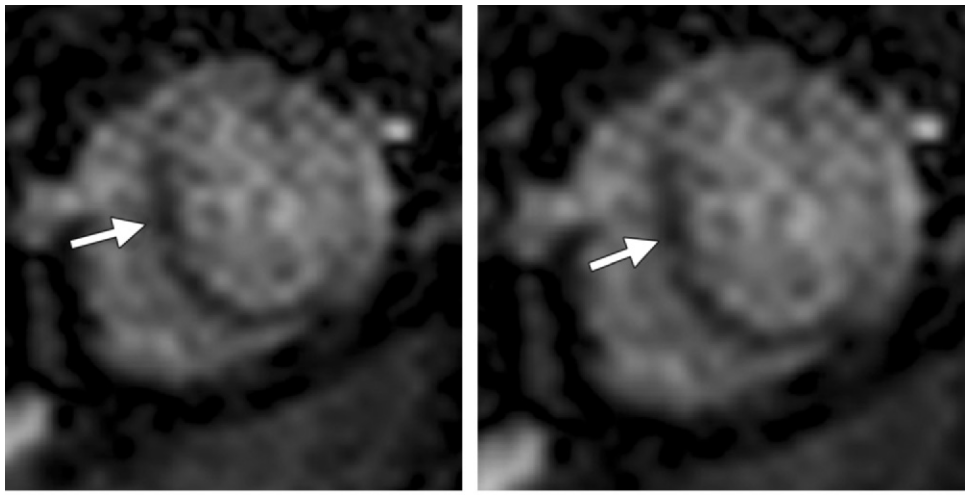

a. b.

Figure 2. MI in perfusion imaging. Stress **(a)** and rest **(b)** MR perfusion images show hypoperfusion involving the septum (arrow) at both stress and rest, consistent with an infarct involving the territory of the left anterior descending coronary artery (LAD).

ischemia, revascularized infarct, or microvascular dysfunction) appear as dark myocardium on the image (Fig 2).

Multisection T1-weighted 2D sequences are typically used for perfusion imaging; these may use SSFP, fast GRE, or GRE with echo-planar readout imaging (EPI) sequences and incorporate inversion-recovery, saturation-recovery, or hybrid preparatory pulses (6). Cine images obtained after infusion of low-dose dobutamine (5–10 μg/kg/min) may be used to evaluate the contractile reserve of myocardium: areas of dysfunctional myocardium that show improved wall thickening with dobutamine indicate the presence of viable myocardium.

T2-weighted black-blood images are used to evaluate the morphology of the heart and pericardium. In MI, T2-weighted imaging is most useful for detecting the presence of edema, which is a marker of acute ischemic injury (7) and enables assessment of the "area at risk." T2-weighted imaging is typically performed using double inversion-recovery FSE with or without fat suppression, in which blood is seen as dark signal and edema is seen as bright signal in the myocardium (8). This technique is prone to artifacts, particularly from the signal produced by slow flow in the diastolic phase or in systolic dysfunction.

Newer techniques for enhancing the sensitivity of T2-weighted imaging include T2-prepared SSFP sequences (9), Acquisition for Cardiac Unified T2 Edema (ACUT2E) turbo spin-echo (TSE)–SSFP sequences (10), and magnetization-prepared SSFP sequences (11). Edema can also be quantified through use of newer T2-mapping techniques, although this use is still relatively early in development (12). Despite these advances, T2-weighted imaging remains subject to artifacts and is a less robust technique than delayed-enhancement imaging.

Early postcontrast T1-weighted fast-GRE images acquired 15 seconds after contrast material administration can be used to detect early hyperenhancement in the myocardium, which is a feature of acute myocarditis, or in the pericardium, which is a feature of acute pericarditis. Microvascular obstruction in acute MI will be seen as a nonenhancing area. Both T2-weighted and early postcontrast images are useful in patients with acute chest pain of uncertain etiology, when the differential diagnosis includes acute pericarditis and acute myocarditis.

Velocity-encoded phase-contrast images acquired perpendicular to the mid–ascending aorta enable quantification of forward and reverse flow in the aorta, from which aortic regurgitation volume and fraction and cardiac output can be calculated. The volumes of the LV and forward flow in the aorta can be integrated to indirectly calculate mitral regurgitant volume and fraction.

3D fat-suppressed whole-heart MR angiographic images acquired in the axial plane are useful for evaluation of proximal coronary arteries, including stenosis and anomalies. On a per-patient basis, the ability of 3D coronary MR angiography to allow categorization of patients

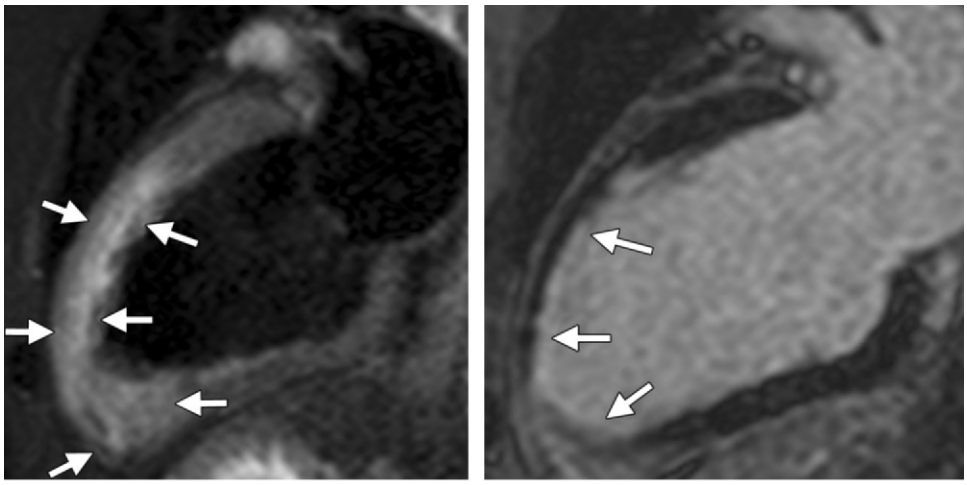

a. b.

Figure 3. MR imaging findings in acute MI in a 34-year-old man with sudden onset of chest pain, elevated cardiac enzymes, and ST-segment elevation. **(a)** Two-chamber T2-weighted short-inversion-time inversion-recovery (STIR) image shows high-signal-intensity edema in the mid and apical anterior wall (arrows), consistent with myocardial edema. **(b)** Two-chamber delayed-enhancement image shows subendocardial scarring in the mid to apical anterior wall (arrows), which is less extensive than the edema seen in **a**; the difference between the two areas defines the myocardial "area at risk" without subsequent revascularization.

with significant obstructive coronary artery disease is not significantly different from that of coronary computed tomography (CT) angiography (13). Nonetheless, the sensitivity and specificity of this sequence, on a per-vessel basis, are lower than those of coronary CT angiography, and to date this technique is typically used less frequently in routine clinical practice.

Real-time cine imaging has poorer spatial and temporal resolution than the standard electrocardiographically (ECG)–gated cine-SSFP sequences. However, it is an effective alternative cine sequence in patients with arrhythmias and those who have difficulty with breath holds. In addition, real-time cine imaging of the ventricular septum is used in diagnosis of pericardial constriction (14).

Regional myocardial function can be accurately quantified with several techniques, including myocardial tagging, phase velocity mapping, strain encoding (SENC), and displacement encoding with stimulated echoes (DENSE) (15). In tissue tagging, saturation bands are applied as lines or grids perpendicular to the myocardium in a specified portion of the cardiac cycle and their deformation over the cardiac cycle is tracked by following the dark lines or intersections; alternatively, information can be obtained directly from the images using optical flow or phase-based techniques such as the harmonic phase (HARP) method.

In phase mapping, velocity is encoded into the phase of the magnetic signal through use of bipolar gradients and calculations of spatial derivatives of velocities in each pixel. In SENC, tag lines are applied parallel to the image plane and strain is calculated based on pixel intensity in subsequent images. With DENSE, in-plane or through-plane tissue displacement is encoded into the phase of an image using radiofrequency pulses and gradients. Regional functions, including strain and velocities, are decreased in infarcted regions (15).

Tagging techniques have also been used to demonstrate the kinetics of remodeling. For example, delayed and prolonged diastolic twisting in patients with anterolateral infarction has been shown to contribute to diastolic dysfunction (16), and persistent elevated wall stresses (reduced shortening) between adjacent and remote noninfarcted regions have been shown to contribute to global dilatation and dysfunction seen in LV remodeling after infarction (17).

MR Imaging Findings in MI

Acute MI

In acute MI, regional wall-motion abnormalities of the affected vascular territory can be seen on cine images. T2-weighted images show wall thickening and myocardial edema (Fig 3a). If there is irreversible damage, hyperenhancement

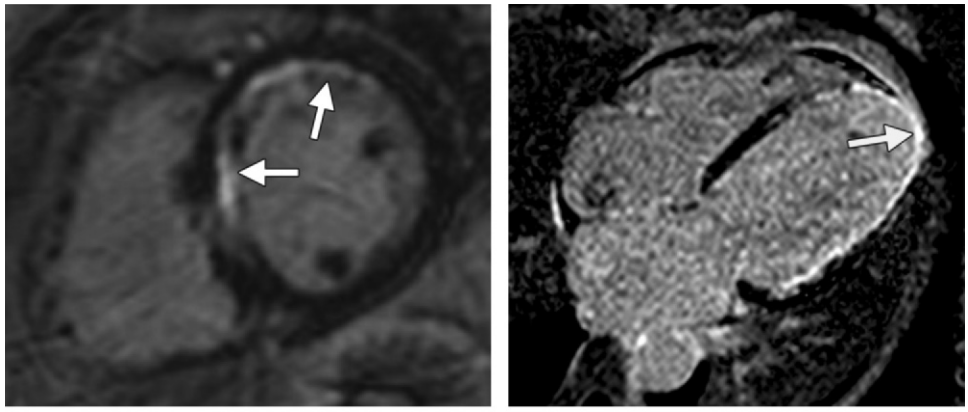

a. b.

Figure 4. Delayed hyperenhancement patterns in MI. **(a)** Short-axis delayed-enhancement image in a 54-year-old man shows a subendocardial pattern of enhancement (arrows) in the midanterior and septal walls, consistent with an infarct in the LAD territory distribution. **(b)** Four-chamber delayed-enhancement image in a 66-year-old woman shows full-thickness transmural delayed hyperenhancement in the apex (arrow) and near-full-thickness delayed hyperenhancement in the lateral wall.

can be seen on delayed-enhancement images along the distribution of the involved epicardial coronary artery due to myocyte death, membrane disintegration or rupture, and intracellular entry of gadolinium (Fig 3b). In addition, the capillary plugging seen in infarcts results in altered wash-in and washout kinetics, with slower uptake and prolonged retention of gadolinium-chelate (3).

If the myocardial damage is partial, subendocardial hyperenhancement can be seen on delayed-enhancement images (Fig 4a), but if the ischemia continues, necrosis gradually progresses outward to involve the epicardium, with ensuing transmural delayed hyperenhancement (Fig 4b). Microvascular obstruction may be present and can be seen as a dark nonenhancing area within the enhancing scar on delayed-enhancement images (Fig 5). Perfusion defects can be seen on rest perfusion images in regions of recently infarcted myocardium. Stress images are not typically obtained in patients with suspected acute coronary syndrome (ACS).

Chronic MI

In established chronic MI, cine images show wall thinning and regional wall-motion abnormalities in the affected territory. Edema is not seen on T2-weighted images. Delayed-enhancement images show wall thinning and subendocardial or transmural delayed hyperenhancement in a vascular distribution. Gadolinium is trapped in the extracellular matrix, resulting in increased volume of distribution (4). Perfusion defects may be seen on both rest and stress perfusion images, depending on the degree of transmurality of irreversibly damaged myocardium.

Figure 5. Microvascular obstruction in a 47-year-old man. Three-chamber delayed-enhancement image shows a full-thickness transmural infarct in the basal inferolateral wall (straight arrow). Within this area of scar, there is a nonenhancing dark focus (curved arrow), consistent with acute microvascular obstruction within an infarct and indicating an area of no-reflow phenomenon.

MR Imaging in Establishing Diagnosis

MR imaging plays an important role in establishing the diagnosis of both acute and chronic MI, although the relative importance of various MR imaging techniques differs. The delayed-enhancement technique has high sensitivity for identification of both acute (99%) and chronic (94%) MI (18), with the ability to detect as little as 1 gram of irreversibly damaged tissue (19). Animal studies have established good correlation between the amount of scar detected with the de-

Teaching Point

Table 4
Differential Diagnosis for ST-Segment Elevation

Acute MI
Acute myocarditis
Acute pericarditis
Takotsubo cardiomyopathy
Left ventricular hypertrophy
Left ventricular aneurysm
Sarcoidosis
Acute aortic dissection
Pulmonary embolism
Arrhythmogenic right ventricular dysplasia
Brugada syndrome
LBBB
Hyperkalemia
Electrical cardioversion
Ventricular paced rhythm
Prinzmetal angina
Benign early repolarization (normal variant)
Osborn wave of hypothermia
Acute cerebral hemorrhage
Normal variant

layed-enhancement technique and histopathology (3,20). The delayed-enhancement technique also has 97% accuracy for prediction of the vascular distribution of the scar (18).

Because of its higher spatial resolution, delayed-enhancement MR imaging has been shown to be superior to single-photon-emission CT (SPECT) in identifying irreversibly damaged myocardium, especially in nonanterior locations, and correlates with enzyme release and positron emission tomography (PET) scans (21). As a result of these advantages, delayed-enhancement MR imaging findings are now being incorporated into diagnostic criteria for imaging patients with MI (20).

Diagnosing Acute MI

MR imaging is usually not required for diagnosis of acute MI, as this condition typically manifests with classic clinical, ECG, and enzyme abnormalities. Acute MI is diagnosed in the setting of ischemic symptoms when there is a characteristic increase and subsequent decrease in troponin or creatine kinase–MB (heart) fraction levels, along with Q waves or ischemic changes at ECG (ST-segment elevation or depression) or coronary artery intervention. However, the clinical presentation of acute MI is variable and occasionally overlaps with that of other conditions that cause myocardial injury; in these cases, MR imaging can be useful for accurate diagnosis.

Teaching Point

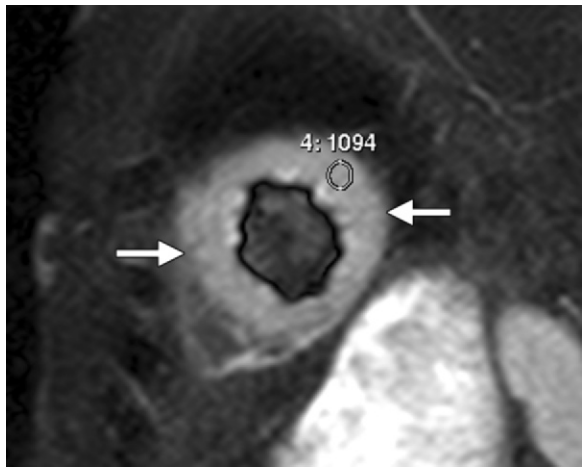

Figure 6. Short-axis T2-weighted STIR image in a 67-year-old woman with acute chest pain and ST-segment elevation shows diffuse myocardial edema (arrows). There was no delayed hyperenhancement (not shown).

MR imaging can also be a useful diagnostic tool in the 10% of patients with suspected STEMI and 32% of patients with ACS who do not have a culprit lesion (21) and the 9.5% who do not have significant coronary artery disease at coronary angiography (22). These angiographic findings could be caused by either transient coronary artery spasm, recanalized coronary artery occlusion, or coronary artery disease in multiple vessels, making it difficult to identify the exact culprit lesion (2). MR imaging is also useful as a diagnostic tool in patients with acute chest pain whose ECG results or cardiac enzyme levels are not suggestive of acute MI.

Normal Coronary Arteries at Angiography: Non–Coronary Artery Disease.—Mild ST-segment elevation can be a normal finding, particularly in men aged 17–24 years, but in healthy patients this mild elevation is not associated with chest pain or abnormal enzyme levels (23). The differential diagnosis for patients presenting with chest pain and ST-segment elevation at ECG and normal or equivocal cardiac enzymes but with normal coronary arteries is shown in Table 4. MR imaging plays an important role in establishing a diagnosis in these patients. Assomull et al (24) found that MR imaging was able to provide clinicians with a diagnosis in 65% of patients with chest pain, elevated cardiac enzymes, and unobstructed coronary arteries. Common causes of these symptoms included myocarditis (31%), takotsubo cardiomyopathy (31%) (Fig 6), and STEMI without an angiographic lesion (29%).

In ischemic etiology with irreversible damage, delayed enhancement is either subendocardial or transmural along the distribution of the culprit epicardial coronary artery. However, MR imaging findings in patients with non–coronary artery disease vary depending on the condition and the type of sequence used. In acute myocarditis, defined as acute inflammation of the myocardium, global or regional systolic dysfunction is seen with cine imaging; early hyperenhancement (hyperemia and capillary leak), delayed hyperenhancement, and edema on T2-weighted images are seen in the midmyocardial or subepicardial layers, typically in the inferolateral or lateral walls, and less commonly in the septum (25).

Takotsubo or stress-induced cardiomyopathy is characterized by transient wall-motion abnormalities in the apical and mid portions of the LV without evidence of coronary obstructive disease (Movie 1 [online]). Edema may be seen on T2-weighted images, but delayed hyperenhancement is not seen (Fig 6). Reverse and atypical patterns of wall-motion abnormalities have also been described (26).

In acute pericarditis, defined as acute inflammation of the pericardium, T2-weighted images show pericardial thickening (>4 mm) and effusion. Images show both early and delayed hyperenhancement, which may extend into the epicardial fat or myocardium (27). Features of pericardial constriction may be seen transiently during the acute attack, including diastolic restraint, abrupt cessation of diastolic filling, tubular deformity of the ventricles, and exaggerated ventricular interdependence, which manifests as exaggerated diastolic septal flattening with inspiration (14).

In patients with hypertrophic cardiomyopathy (HCM), who present rarely with acute chest pain and an abnormal ECG, delayed-enhancement MR imaging shows asymmetric LV hypertrophy and patchy areas of sand-like hyperenhancement, particularly at the superior and inferior RV insertion points (28).

Cardiac sarcoidosis is seen in ~25% of sarcoidosis patients without known cardiac disease (29,30). In the acute phase, T2-weighted MR imaging shows myocardial thickening and edema, associated with patchy delayed hyperenhancement in subepicardial or midmyocardial layers (29,30).

Patients with acute aortic dissection typically present with chest pain without elevation of cardiac enzymes but occasionally with ST-segment elevation at ECG. MR imaging shows the dissection flap on cine SSFP or angiographic images (31).

Pulmonary embolism can rarely lead to ST-segment elevation, T-wave inversion, and acute chest pain. CT angiography is most commonly used for diagnosis of this condition, but MR angiography can also be used (32).

Finally, arrhythmogenic RV dysplasia is a rare cause of chest pain and ST-segment elevation. In patients with arrhythmogenic RV dysplasia, MR imaging shows fat infiltration of RV myocardium on T2-weighted images; RV dilatation, focal aneurysms, and global and regional wall-motion abnormalities on cine images; and scarring on delayed-enhancement images, particularly in the anterobasal RV wall and RV outflow tract (33).

Normal Coronary Arteries at Angiography: Recanalization of Coronary Arteries.—Results of coronary angiography may be normal in a patient with elevated enzyme levels and ECG changes caused by spontaneous recanalization of a diseased coronary artery or by transient events not associated with coronary artery disease, such as embolism with spontaneous lysis of thrombus or coronary vasospasm. In these scenarios, MR imaging is useful for excluding any non–coronary artery diseases. The presence of an ischemic pattern of delayed hyperenhancement establishes MI as the cause of chest pain, and the absence of a culprit lesion at coronary angiography could be explained by one of the preceding reasons (recanalization, embolus, or vasospasm).

Multivessel Coronary Disease at Angiography: Difficulty in Establishing Culprit Lesion.—In this scenario, an acute MI can be diagnosed when edema is seen on T2-weighted images and scarring is seen on delayed-enhancement images. Based on the distribution of these abnormalities, the culprit lesion can be established and therapy can be appropriately targeted (Fig 7).

Establishing Diagnosis before Angiography.—Chest pain, ECG changes, and abnormal enzyme levels are highly suggestive though not specific for a diagnosis of acute MI. The new imaging criteria for diagnosis of acute MI include new wall-motion abnormality at echocardiography and loss of viable segment at another imaging modality, such as myocardial perfusion imaging by nuclear medicine (2). Neither of these criteria is sensitive or specific enough to allow definitive identification of MI: new wall-motion abnormality occurs only when >30% of myocardium is infarcted, and loss of viable myocardium can be detected with nuclear medicine only when >10 grams is infarcted. In addition, these findings can also be seen in patients with ischemia without infarction and in those with nonischemic conditions such as inflammation.

Figure 7. Infarction in different vascular territories. **(a, b)** Two-chamber **(a)** and short-axis **(b)** delayed-enhancement images show near-full-thickness to full-thickness delayed hyperenhancement in the basal, mid, and apical anterior and anteroseptal segments (arrows), in an LAD territory distribution. **(c, d)** Three-chamber **(c)** and short-axis **(d)** delayed-enhancement images in another patient show transmural hyperenhancement in the basal and midinferolateral and inferior segments (arrows), consistent with an infarct in the left circumflex coronary artery (LCX) territory. **(e)** Short-axis delayed-enhancement image in another patient shows a full-thickness and near-full-thickness transmural scar in the midinferior and inferoseptal segments (arrows). In addition, a near-full-thickness scar is also seen in the right ventricular wall (arrowheads). These findings are consistent with an infarct in the right coronary artery (RCA) territory.

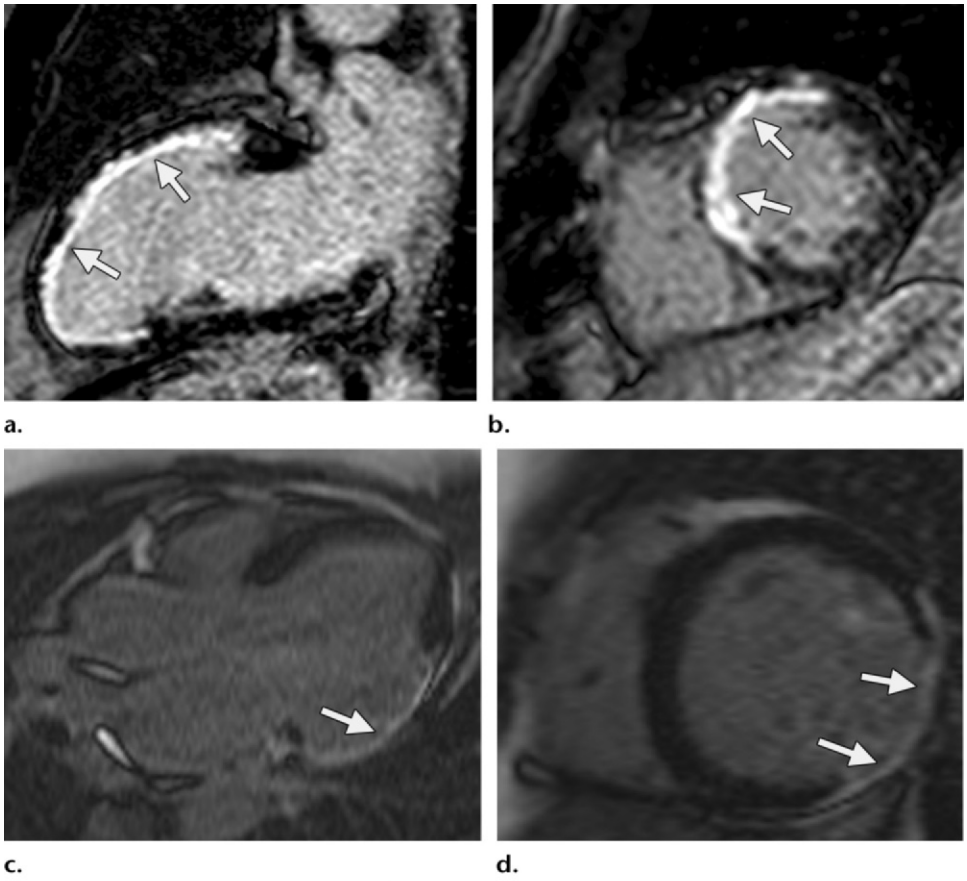

Because MR imaging has high sensitivity and accuracy for detection of even small and subendocardial scars, it is particularly useful for establishing a diagnosis of acute MI. A recent study has shown that adding MR imaging to the conventional tests enhances the accuracy of MI diagnosis (34). In addition, use of MR imaging may allow clinicians to diagnose MI before troponin levels are elevated (35).

Diagnosing Chronic MI

MR imaging plays an important role in establishing a diagnosis of chronic MI and distinguishing this condition from other nonischemic cardiomyopathies, particularly in the setting of congestive cardiac failure. A large subset of patients presenting with congestive cardiac failure are diagnosed with dilated or nondilated cardiomyopathy based on echocardiography results; coronary artery disease accounts for 62% of congestive cardiac failure cases (36). Identifying the specific cause of cardiomyopathy is essential for determining prognosis

Teaching Point

Figure 8. Ischemic and nonischemic patterns of delayed hyperenhancement in MR imaging. **(a)** Ischemic enhancement is subendocardial to transmural in a vascular distribution. **(b)** Nonischemic enhancement may be midmyocardial, subepicardial, or diffuse subendocardial. Midmyocardial enhancement may be linear, patchy, or at the RV insertion points of the interventricular septum. *DCM* = dilated cardiomyopathy, *HE* = hyperenhancement.

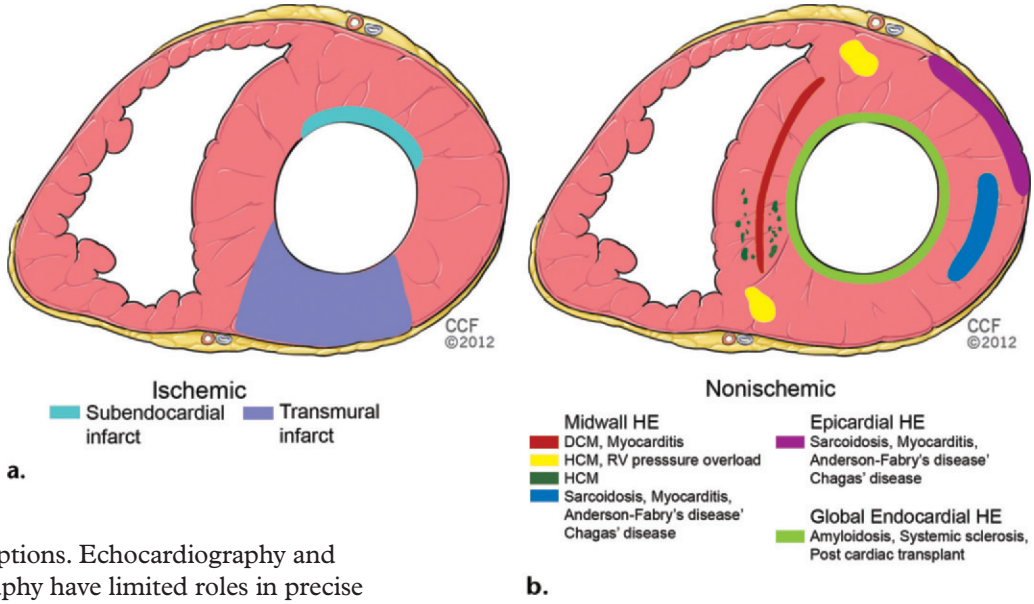

and treatment options. Echocardiography and nuclear scintigraphy have limited roles in precise etiologic determination in patients with congestive heart failure, as the imaging appearances of the LV may be nonspecific. In addition, endomyocardial biopsy is not sensitive for etiologic determination, as it is hindered by sampling error (37).

As discussed earlier, delayed-enhancement MR imaging is ideally suited for detection and characterization of ischemic and nonischemic etiologies. Ischemic pattern scarring in patients with chronic MI is either subendocardial or transmural in a vascular territory distribution (Fig 8a). In one MR imaging study that used delayed enhancement, 13% of patients with a diagnosis of dilated cardiomyopathy had ischemic scarring (38).

Delayed hyperenhancement is also seen in various nonischemic diseases that cause cardiac failure; an analysis of the pattern and location of delayed hyperenhancement in these patients should allow clinicians to narrow the differential diagnosis. The patterns of hyperenhancement for nonischemic conditions are midmyocardial (linear, patchy, or at the RV insertion points), subepicardial (or epicardial), and global subendocardial or transmural (39) (Fig 8b) (Table 5). Diseases associated with these patterns of enhancement include nonischemic dilated cardiomyopathy (Fig 9a), myocarditis (Fig 9b), sarcoidosis (Fig 9c), HCM (Fig 9d), amyloidosis, endocardial fibroelastosis, Fabry disease, systemic sclerosis, and Chagas disease. Detection of scarring on delayed-enhancement images, whether ischemic or nonischemic in pattern, is important, as even a small amount of scarring can adversely affect a patient's prognosis.

In patients with cardiac failure, coronary angiography should be performed to exclude coronary artery disease. Clinicians should recognize that negative results at coronary angiography do not allow exclusion of ischemia as a cause of heart failure, as there could have been spontaneous recanalization after occlusion; in these cases, MR imaging can be useful for diagnosis, as an ischemic pattern of enhancement will be present. Clinicians should also remember that absence of scarring in a patient with severe systolic dysfunction does not allow complete exclusion of coronary artery disease: no scarring is seen in coronary artery disease with globally hibernating myocardium. Delayed-enhancement MR imaging has high sensitivity for detection of underlying coronary artery disease in patients with poor LV function, as well as complications such as thrombus and aneurysm, which occasionally can be asymptomatic (37).

Diagnosing Iatrogenic MI

Iatrogenic infarcts may be caused intentionally in the septum after septal artery alcohol ablation for HCM (Fig 10) or after ablation of an arrhythmogenic focus. In these cases, myocardial edema is seen on T2-weighted images immediately after the procedure; microvascular obstruction and delayed hyperenhancement can be observed in the ablated area. The extent of enhancement after ablation has

Table 5
Various Patterns of Delayed Hyperenhancement in Cardiac MR Imaging

Category	Pattern	Associated Entities
Ischemic	Subendocardial transmural	MI
Nonischemic	Midmyocardial	
	Linear septal	Dilated cardiomyopathy, myocarditis
	Patchy	Myocarditis, sarcoidosis, Fabry disease, Chagas disease
	Patchy at RV insertion point	HCM, RV pressure overload, systemic sclerosis
	Epicardial	Myocarditis, sarcoidosis, Fabry disease, Chagas disease
	Global subendocardial	Amyloidosis, endocardial fibroelastosis, systemic sclerosis, cardiac transplantation, uremia

Figure 9. Nonischemic patterns of delayed hyperenhancement in MR imaging. **(a)** Short-axis delayed-enhancement image in a 65-year-old man with LV dysfunction shows a dilated LV with a linear midmyocardial pattern of enhancement (arrow), which is typical of nonischemic dilated cardiomyopathy. Results of coronary angiography were normal. **(b)** Three-chamber delayed-enhancement image in a 43-year-old man shows a patchy midmyocardial and subepicardial pattern of hyperenhancement (arrow) in the basal inferolateral segment. High signal intensity was seen on T2-weighted images (not shown), consistent with acute myocarditis. **(c)** Short-axis delayed-enhancement image in a 69-year-old man with known systemic sarcoidosis shows a diffuse myoepicardial scar in the LV (arrows), consistent with cardiac sarcoidosis. The diagnosis was confirmed with endomyocardial biopsy. **(d)** Short-axis delayed-enhancement image in a patient with HCM shows patchy areas of hyperenhancement (arrows) in the LV myocardium, particularly at the RV insertion sites of the interventricular septum.

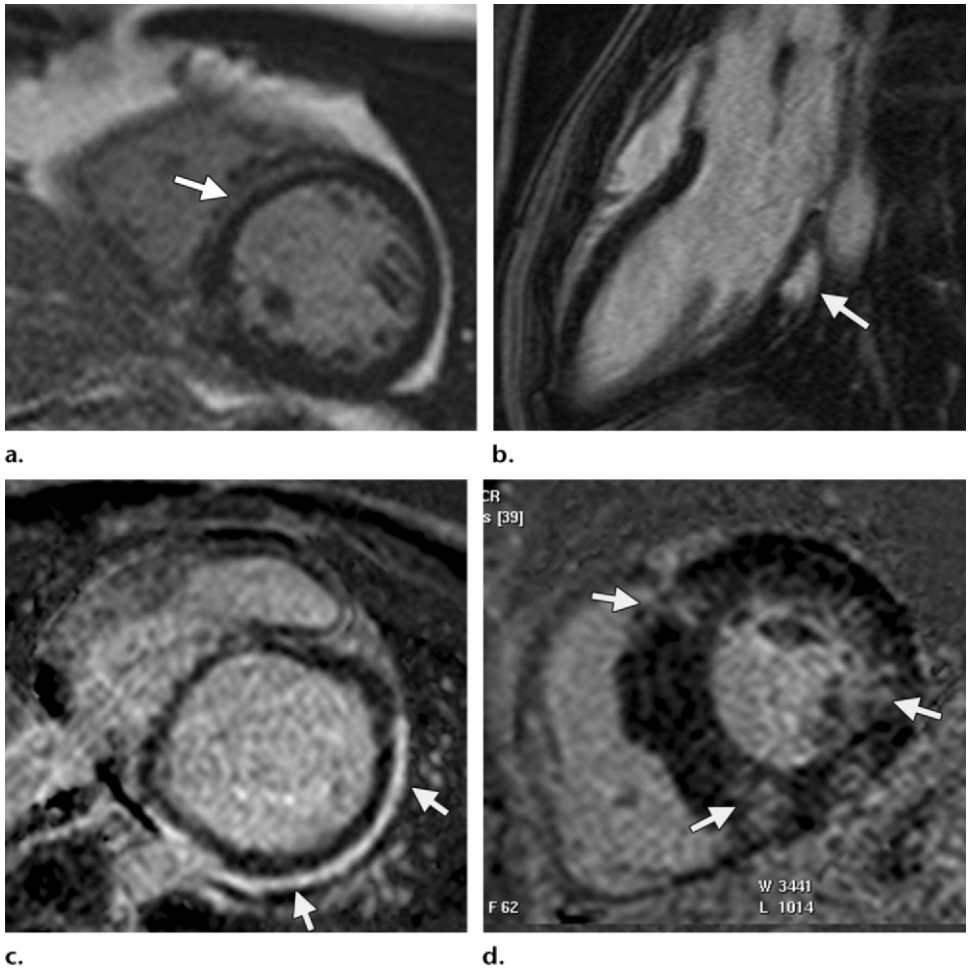

been shown to be directly correlated with the reduction of pressure gradient in HCM (40).

Iatrogenic infarcts can also be caused unintentionally after revascularization or other cardiac procedures. These infarcts are usually well-defined and focal within the territory of intervention (19).

MR Imaging in Determining Age of Infarct

In addition to being useful as a diagnostic tool, MR imaging can also be used to distinguish acute and chronic infarcts, which is particularly helpful when a patient has multiple infarcts in various vascular territories or when an infarct is discovered in the absence of clinical symptoms. Because the two types of infarcts are managed differently, establishing the infarct age is crucial. Both acute and chronic infarcts may be associated with wall-motion abnormalities, perfusion defects, and scarring; these characteristics are therefore not definitive in differentiating between infarct types. Although wall thickening is a feature of acute MI and wall thinning a feature of chronic MI, these findings are not specific to either diagnosis. Microvascular obstruction is characteristic of acute MI, but is seen in at most 50% of these cases (7).

T2-weighted imaging is the most useful sequence for determining the age of an infarct. Edema on T2-weighted images is seen only in acute MI. This also allows determination of an acute infarct in a patient with mixed acute and chronic MI. Similar findings have been seen on postcontrast cine SSFP images as a result of the T2/T1-weighting component of SSFP images (41).

MR Imaging in Risk Stratification and Prognostic Indicators

Extensive research on MI over the past 10 years has resulted in identification of a variety of prognostic indicators that enable risk stratification.

Acute MI

Reversible versus Irreversible Injury.—Contrast MR imaging alows differentiation of reversible from irreversible injury, independent of wall motion and infarct age (3). Delayed hyperenhancement of myocardium indicates irreversible injury for both acute and chronic MI; myocardial edema on T2-weighted images indicates acute MI.

The area of edema shown on T2-weighted images is consistently larger than the area of irreversible necrosis shown on delayed-enhancement images (8). Subtracting the area of delayed hyperenhancement from the area of edema provides an estimation of the "salvageable area" (ie, the area at risk) (42), the area that can be salvaged or has been salvaged by revascularization (43,44). This area can be measured retrospectively after the revascularization procedure. The myocardial salvage index (MSI) (T2-weighted area − delayed-enhancement area/T2-weighted area) has a prognostic value with high sensitivity and specificity, with values similar to those seen based on infarct size or area of microvascular obstruction (44). However, use of T2-weighted imaging to determine areas at risk is not universally accepted due to inadequate validation studies and limited contrast between normal and abnormal areas (45).

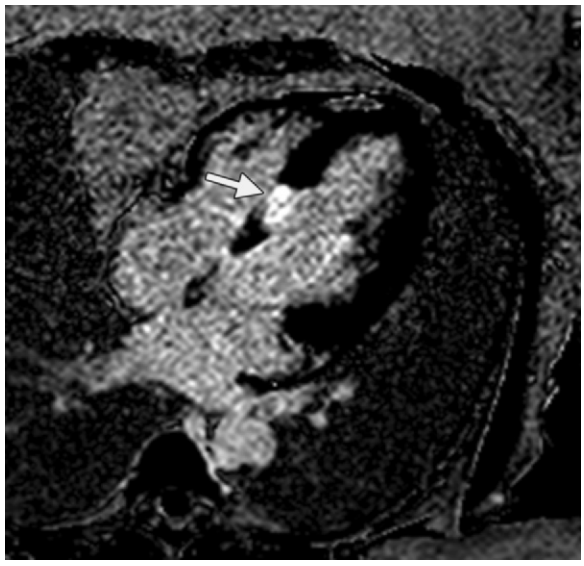

Figure 10. Four-chamber delayed-enhancement image in a patient with a history of alcohol ablation for HCM shows full-thickness hyperenhancement in the basal septal wall (arrow), consistent with alcohol ablation–induced scarring.

Transmurality.—Transmurality of the infarct has an independent prognostic value in determining the recovery of contractile function after therapy (3). There is an inverse relationship between the transmural extent of MI and the recovery of segmental contractile function after revascularization: a greater transmural extent is associated with poorer recovery (46,47). Delayed-enhancement MR imaging is the most accurate method for identifying transmurality because of the technique's high spatial and contrast resolution (3). Transmural infarcts are associated with poor recovery (3).

Microvascular Obstruction.—Microvascular obstruction or "no-reflow" phenomenon is seen in acute MI and indicates a failure to reperfuse a

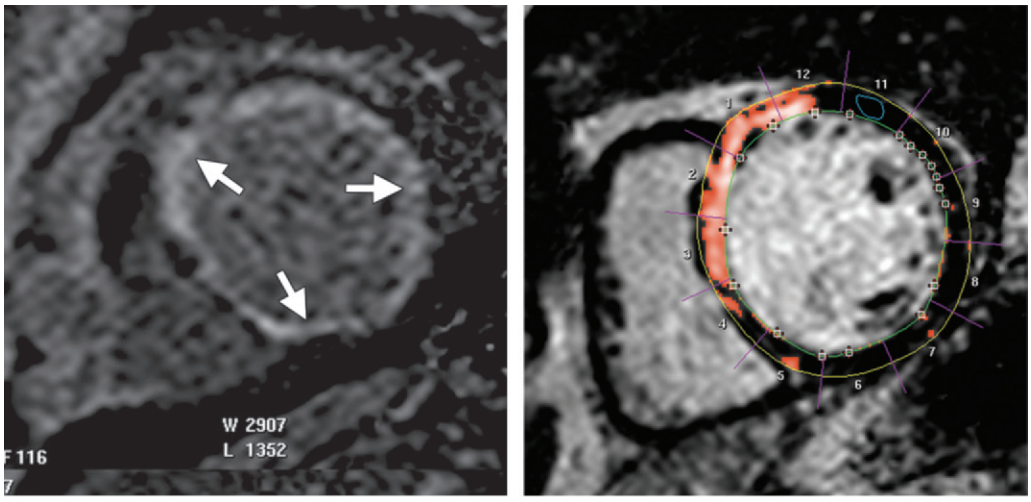

a. b.

Figure 11. **(a)** Short-axis delayed-enhancement image in a 72-year-old man shows extensive infarct in all vascular territories (arrows), which is associated with poor success after revascularization. **(b)** Short-axis delayed-enhancement image in a patient with chronic MI in the midanterior and anteroseptal segments. The threshold value is generated from normal myocardium (blue outline) in the anterolateral wall. Tissues with signal intensity >2 standard deviations over this normal value are labeled as infarct and can be quantified (red pixels).

portion of myocardium despite re-establishment of epicardial coronary-artery patency. At MR imaging, microvascular obstruction is seen in the presence of severe microcirculatory damage, which results from myocyte death, spilling of intracellular contents, and severe sludging and occlusion of end-arteries and capillaries. Microvascular obstruction indicates severe ischemic disease (typically transmural MI) and is associated with poorer prognosis, adverse cardiovascular events, and adverse remodeling (48,49).

Because of the lack of blood flow to the necrotic core, gadolinium does not reach the center of the infarcted zone; therefore, no T1 shortening occurs, resulting in a dark signal. This can be seen with first-pass perfusion imaging and early- or delayed-enhancement imaging. Although a greater degree of microvascular obstruction is detected with first-pass imaging, delayed-enhancement imaging has greater spatial resolution and the highest contrast-to-noise ratio for detection of microvascular obstruction. In addition, microvascular obstruction detected with delayed-enhancement imaging is the strongest prognostic marker for adverse ventricular remodeling (50) and the most powerful predictor of global and segmental functional recovery, providing further incremental value to the transmural extent of infarction (50).

The presence of microvascular obstruction on early delayed-enhancement images has also been shown to be associated with adverse LV remodeling and adverse cardiovascular events (49). If delayed-enhancement imaging is performed 40 minutes after gadolinium-chelate administration, the necrotic core may show contrast material uptake primarily caused by slow diffusion of contrast material, not perfusion (51).

Chronic MI

Scar Size.—The extent of infarct is inversely proportional to the prognosis (52): the likelihood of recovery is lower if ≥50% of the myocardium is involved in the infarcted segment (Fig 11a). Scarring predicts adverse LV remodeling after infarction (53,54). In addition, infarct size is a better predictor of ventricular tachycardia than LV ejection fraction or volumes, as scars are a substrate for arrhythmia (55,56). Scar size as assessed with MR imaging can predict survival and all-cause mortality independent of LV ejection fraction (57–59). Delayed-enhancement MR imaging is highly accurate in measuring scar size (3,60); this accuracy has reduced the sample size required for various clinical trials (21).

Measurement of infarct size in the first few days after occlusion may overestimate the size because of edema and cellular elements (61). The infarct size is the largest in the first 7–10 days after acute injury due to tissue expansion from edema. With time, the size of the infarct

decreases as a result of resolution of tissue edema and gradual contraction of the resultant scar tissue (by as much as 25% over a period of 4–8 weeks) (62). Moreover, the mass of the remaining myocardium may also increase over time because of compensatory hypertrophy; as a result, the scar percentage appears to become smaller, although this change may not be reflected in measurements of LV total volume and mass.

Various techniques are used to measure the MI scar. The first technique is the qualitative method. With this technique, the scar in each of the 17 standardized myocardial segments (63) is visually scored with a five-point scale: 0 = no hyperenhancement, 1 = 1%–25% hyperenhancement, 2 = 26%–50% hyperenhancement, 3 = 51%–75% hyperenhancement, and 4 = 76%–100% hyperenhancement. A summed scar score can then be obtained by summing the score of each segment and dividing by 17. Alternatively, each regional score can be weighted by the midpoint of the enhancement range (1 = 13%, 2 = 38%, 3 = 63%, and 4 = 88%) and the score can then be divided by 17 (18). The transmurality index, as mentioned earlier, can be obtained by counting the number of segments with a score of 3 or 4 and dividing by 17.

The second technique for measuring the MI scar is the semiquantitative thresholding method. With this technique, scar is defined as tissue with a signal intensity 2–3 standard deviations above the mean signal intensity of remote normal myocardium. Based on this definition, the computer automatically calculates the scarred areas of the myocardium (Fig 11b). Although this technique has been demonstrated to be accurate in animal studies with high spatial resolution and no motion (64), this method has demonstrated less accuracy in clinical studies, likely as a result of motion and partial-volume effects, which produce a gray area of mixed viable and nonviable cells (64).

To avoid overestimation, a threshold of 6 standard deviations (instead of 2–3 standard deviations) has been used for scar detection (62,64,65). Other techniques used for semiquantitative thresholding include the full width at half maximum method, which uses 50% of the maximum intensity of infarct as the threshold for scar (66); weighting to each voxel (67); and using a combination of methods (68). These techniques are not completely objective, as the normal tissue is determined by the observer and could be either false-positive (noise) or false-negative (microvascular obstruction).

The third technique for measuring MI scar is manual planimetry, in which the areas of hyperenhancement are subjectively determined by an observer, manually contoured, and then expressed as grams or as a percentage of the total cardiac mass.

Missed Infarcts.—Approximately 40%–60% of MIs are silent and unrecognized (69). Silent MI is associated with a six- to 11-fold increased risk of major cardiac events and a worse prognosis (69). The presence of even a small scar in patients without a history of MI is associated with a high risk of adverse events. Although Q waves at ECG can be an indicator of previous infarct, this measurement is neither sensitive nor specific: MI can occur without abnormal Q waves, and Q waves can be seen in nonischemic patients (21). Therefore, MR imaging can be a useful tool for diagnosing a silent MI, particularly when Q waves are not present. Delayed-enhancement MR imaging has been shown to allow identification of silent MI 76%–390% more frequently than ECG (69,70).

Teaching Point

Other Prognostic Indicators

Hemorrhage in Core of Infarct.—Hemorrhage is seen in the core of an infarct in up to 25% of patients with MI, particularly those with reperfused infarcts. This hemorrhage appears on T2-weighted images as a dark area because of hemosiderin produced by hemoglobin degradation (71). Hemorrhage within the core has been shown to be an adverse prognostic indicator that is associated with adverse LV remodeling, large infarct size, increased LV end-systolic volume, and no improvement in ejection fraction over time (72).

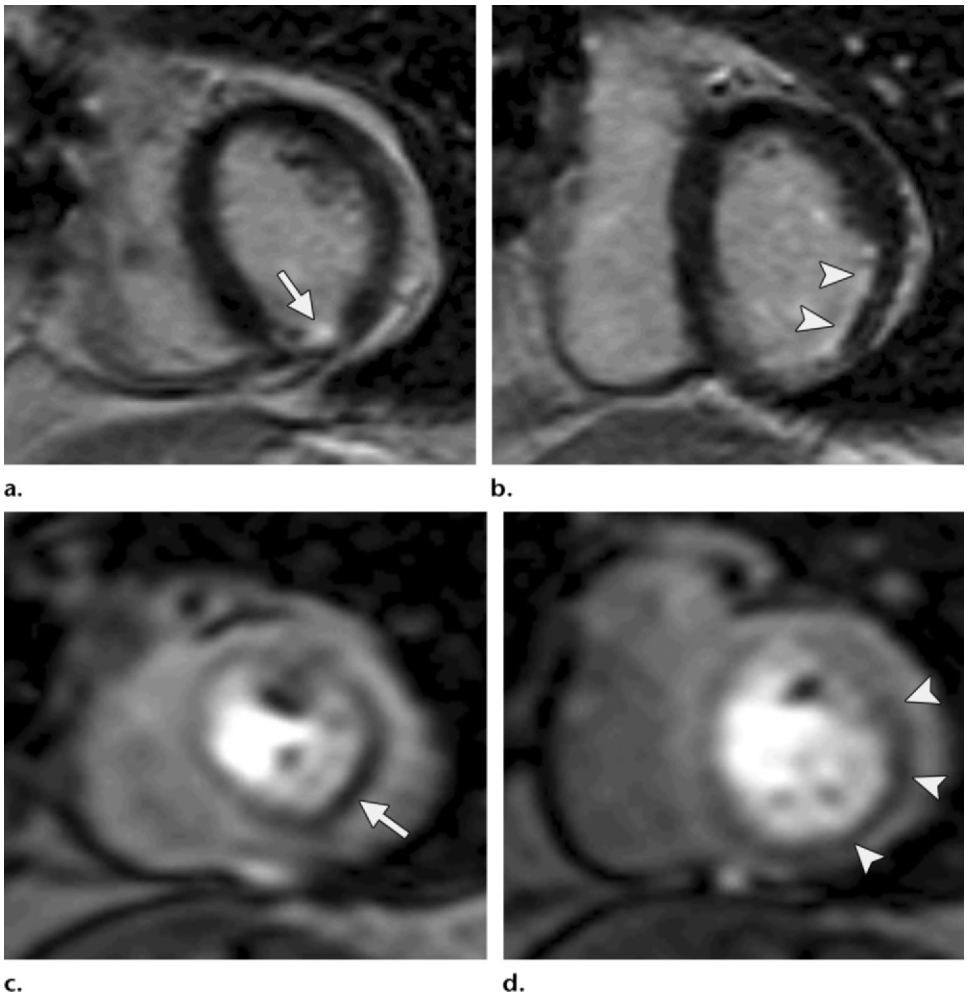

Figure 12. Peri-infarct ischemia. **(a, b)** Short-axis delayed-enhancement images from the midventricle **(a)** and base **(b)** show focal near-transmural infarction in the inferior wall (arrow in **a**) and subendocardial infarction in the inferior and inferolateral walls (arrowheads in **b**). **(c, d)** Short-axis stress perfusion images from the same midventricular **(c)** and basal **(d)** section positions show hypoperfusion (ischemia) (arrow in **c**, arrowheads in **d**) adjacent to and of greater extent than the noted myocardial scar seen on the delayed-enhancement images, indicative of peri-infarct ischemia.

Ischemia.—Ischemia is characterized by perfusion defects on stress images and normal rest images (Fig 12). In a multicenter study, MR imaging was found to be highly accurate for detecting obstructive coronary artery disease, with 91% sensitivity and 81% specificity when compared with angiography. The diagnostic performance of MR imaging was also found to be at least equal to that of SPECT in a large multicenter trial (5) and superior to that of SPECT in a recent large single-center trial (73). The presence of ischemia in suspected coronary artery disease allows identification of individuals at high risk of cardiac death, nonfatal MI, or congestive heart failure. In patients with severe ischemic cardiomyopathy, the presence of peri-infarct ischemia is associated with a higher incidence of cardiovascular events than in those without peri-infarct ischemia (74).

Other Indicators.—The extent of the peri-infarct zone is related to all-cause mortality. Higher infarct or peri-infarct heterogeneity correlates with increased ventricular irritability, susceptibility to ventricular tachycardia, and all-cause mortality (56). In addition, RV function—as assessed with cine imaging—late after MI is an important prognostic indicator (21). MR imaging is superior to echocardiography in evaluation of RV function (21).

Strain rates obtained with SENC have been shown to predict persistent severe myocardial dysfunction at follow-up of MI; these rates may therefore serve as a potential parameter for determining viability (75). In addition, SENC may be useful in identifying subtle old infarcts and distinguishing between subendocardial and transmural infarcts based on a difference in strain values (15).

MR Imaging in Predicting Response to Therapy

Treatment of MI and its complications often involves use of surgical or interventional procedures that are associated with high cost and high morbidity and mortality rates, making proper patient selection vital. MR imaging can provide information that will improve patient selection for these procedures.

Revascularization

The most important predictor of successful outcome after a revascularization procedure such as coronary artery bypass grafting is the presence of scarring. There is an inverse relationship between the extent of scar and the recovery of contractile function (46).

MR imaging allows distinction of dysfunctional myocardium with reversible myocardial dysfunction, such as stunning or hibernation, from irreversible stages such as infarction. Myocardial stunning occurs when an acute, transient ischemic insult results in contractile dysfunction that persists despite restoration of coronary blood flow. Myocardial hibernation can occur as a result of a prolonged period of stunning, secondary to repetitive stunning events, or from chronically reduced coronary blood flow and oxygen supply. Viable myocardial cells may adapt to reduced oxygen supply by decreasing their contractile function (down-regulation), although these cells retain the potential for contractile recovery after restoration of coronary blood flow.

Delayed-enhancement MR imaging allows detection of viable segments that may benefit from revascularization. Normal wall motion and lack of hyperenhancement suggest normal tissue, whereas a combination of wall-motion abnormality and >75% segmental hyperenhancement suggests nonviable infarcted tissue with little to no potential for functional improvement after revascularization. Wall-motion abnormality with no or minimal (<25%) hyperenhancement suggests dysfunctional but viable myocardial tissue with a high likelihood of functional improvement or recovery after revascularization. Segments that are dysfunctional and have intermediate degrees of hyperenhancement (25%–75%) have correspondingly intermediate potential for functional recovery (Table 6) (3).

Viability can be assessed with various modalities, including SPECT, PET, dobutamine echocardiography, CT, and MR imaging (Table 7) (76–79). SPECT can be performed with either thallium-201 or Tc-99m sestamibi using either pharmacologic or physiologic stress. With this technique, delayed uptake in areas of perfusion defect indicates viable myocardium: thallium uptake depends on energy-dependent transport, whereas sestamibi uptake depends on active mitochondria. Retention of the isotope 4 hours after injection depends on the integrity of the cell membrane and viability.

With PET, uptake of ^{18}F FDG in the myocardium in a segment with reduced perfusion on rubidium-82 or nitrogen-13 ammonia PET scans indicates viable myocardium, as ischemic myocardium preferentially metabolizes glucose over fatty acids. Perfusion scanning can be performed in less than 30 minutes, whereas FDG PET can take up to 4 hours (80).

With dobutamine echocardiography, viable myocardium is seen as dysfunctional myocardium with augmented contractility after stress (known as contractile reserve) (80). However,

Table 6
MR Imaging Features That Enable Differentiation of Various Types of Ischemic Insult to the Myocardium

Myocardial Condition	Wall Motion	Scarring
Normal	Normal	None
Hibernating	Impaired	None
Infarction	Impaired	Present
Viable: high likelihood of recovery	Impaired	<25%
Viable: intermediate likelihood of recovery	Impaired	25%–75%
Nonviable	Impaired	>75%

Table 7
Performance of Various Imaging Modalities in Assessing Myocardial Viability

Imaging Technique	Sensitivity (%)	Specificity (%)
Tc-99m sestamibi SPECT	83*	69*
^{18}F FDG PET	88*	73*
Dobutamine echocardiography	84*	81*
Dobutamine MR imaging	88†	87†
Viability MR imaging	96‡	84‡
CT	77§	97§

Note.—FDG = fluorine-18 fluorodeoxyglucose, Tc-99m = technetium-99m.
*Reference 76.
†Reference 77.
‡Reference 78.
§Reference 79.

echocardiography is operator dependent and may be limited by acoustic windows in large patients and those with chronic obstructive pulmonary disease (COPD). MR imaging can also be used to estimate contractile reserve (77), which can provide additional information in areas with nontransmural scar (20).

Delayed enhancement can also be evaluated with CT (81), but this technique is associated with ionizing radiation and low signal-to-noise and contrast-to-noise ratios (82). A novel technique to improve contrast resolution is to use dual-energy CT and merge morphologic delayed-enhancement images with a dual-energy iodine map (79,83). Of all these techniques, MR imaging has the highest spatial resolution (76,82).

Resynchronization Therapy

Cardiac resynchronization therapy relieves symptoms of cardiac failure by synchronizing the RV and LV contractions, which improves the efficiency of ventricular ejection. In this procedure, a pacemaker lead is placed through a coronary vein to lie adjacent to the lateral wall of the LV, in addition to the usual leads in the right atrium and RV, so that the ventricles can be triggered to contract synchronously. This procedure will not be effective if there is extensive scarring in the lateral wall or septum that prevents electrical activation (84).

Delayed-enhancement imaging allows identification of the amount of scar in the lateral wall

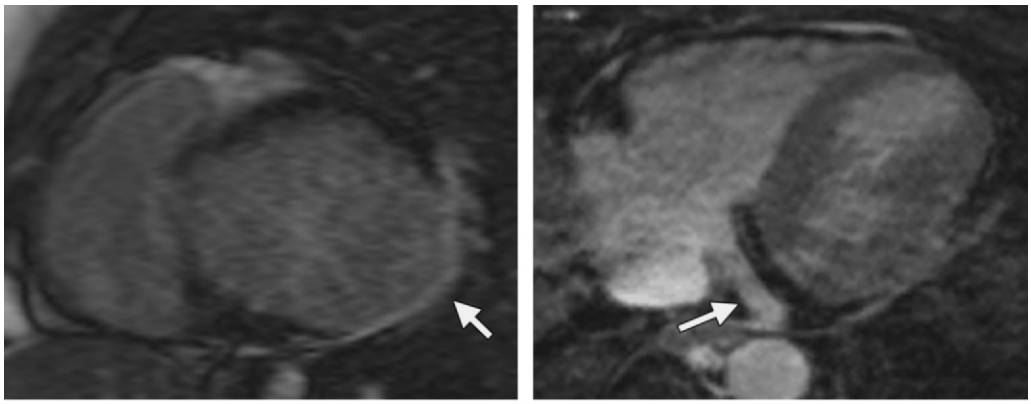

a. b.

Figure 13. MR imaging in cardiac resynchronization therapy. **(a)** Short-axis delayed-enhancement image in a 47-year-old man being considered for cardiac resynchronization therapy shows extensive full-thickness transmural scarring in the anterolateral and inferolateral segments (arrow), which is associated with poor response after cardiac resynchronization therapy. **(b)** Image from 3D whole-heart coronary venography shows the venous anatomy of the heart, which is useful in planning coronary resynchronization therapy. Arrow = coronary sinus.

and the precise anatomic extent of infarcted segments (Fig 13a). 3D whole-heart MR venography can be used to assess the venous anatomy, as variations in venous anatomy (including absence of common veins) may result in failure of the procedure (Fig 13b) (84).

MR Imaging in Detecting Complications of MI

Various complications may develop after MI, particularly when treatment is delayed or inadequate. Symptoms related to the complication may be the first presentation if the infarct was silent, although complications also may be asymptomatic. In either setting, MR imaging is a useful tool for evaluation of complications secondary to MI.

Free-Wall Rupture

Myocardial rupture is seen in 10%–20% of infarcts (85). Rupture is more common in the free wall than in the septum and more common in the LV than in the RV, with the apex being the most common site. Papillary muscle and the ventricular septum are less commonly involved. Myocardial rupture is more common in the first 1–4 days after an MI, when the wall is weakest because of coagulation necrosis and neutrophil infiltration.

Patients at increased risk include those experiencing their first MI; patients who are female; those ≥60 years of age; those with multivessel disease, transmural infarct involving 20% of the wall, poor collateral supply, or absence of ventricular hypertrophy; and those who experienced delayed initiation of thrombolytics (85). In these patients, delayed-enhancement MR imaging shows loss of continuity of the myocardium with irregular margins, with or without a hematoma. Treatment can include surgery, hemodynamic monitoring, and medical therapy with β-blockers and angiotensin-converting enzyme (ACE) inhibitors.

Ventricular Septal Rupture

Ventricular septal rupture is rare, occurring in only 2% of patients with infarct. It is typically seen 2–8 days after an MI and is often lethal (85). A simple rupture is seen as a well-defined defect in the septum, is typically located at the apex, and is more common in anterior MI. A complex rupture has irregular margins with extensive hemorrhage and is more common in the basal inferior septum.

Cine MR imaging can demonstrate the presence of a defect, and velocity-encoded phase-contrast MR imaging allows quantification of the shunt across the defect, either directly or indirectly. Ventricular septal rupture precipitates cardiogenic shock and requires emergency surgery with ventricular-septal-defect patch repair and coronary artery bypass grafting. Both cine and delayed-enhancement MR imaging can then be used to evaluate the adequacy of the repair.

Aneurysm or Pseudoaneurysm

Aneurysm of the LV is seen in 12% of patients after MI (86) and can be either true or false (pseudoaneurysm). True LV aneurysm is a saccular protrusion of the LV wall caused by a mechanically weak, necrotic, or scarred or fibrotic wall. True LV aneurysm is seen in 8%–15% of patients with healed transmural MI (87) and is more common in the anterior and apical walls

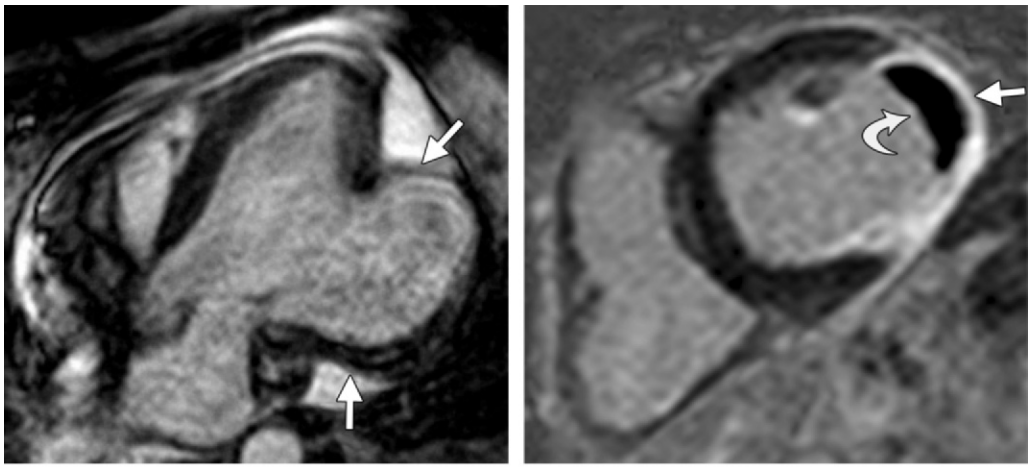

a. b.

Figure 14. **(a)** Four-chamber SSFP image in a 75-year-old man with recent MI shows a wide-mouthed true aneurysm in the lateral wall (arrows). **(b)** Short-axis delayed-enhancement image in a 74-year-old man with recent MI shows scar in the lateral wall of a true LV aneurysm (straight arrow), which is filled with nonenhancing dark thrombus (curved arrow).

Figure 15. Three-chamber delayed-enhancement image shows a large pseudoaneurysm (arrows) originating from the basal and midinferolateral wall of the LV.

(70%–85%). A higher prevalence is seen in patients with anterior infarct; female patients; those with no previous angina; patients with total occlusion of the LAD or absence of infarct-related collateral arteries; and those who experienced delayed initiation of thrombolytics (86).

A true aneurysm has a wide mouth and is akinetic or dyskinetic during systole. In patients with true aneurysm, delayed hyperenhancement may be seen because of scarring (Fig 14). Thrombus is seen within 50% of aneurysms, and calcification of the wall and thrombus may be present (although calcification is better seen with radiography or CT). Aneurysm can result in heart failure, ventricular arrhythmias, or thromboembolism (87,88). Treatment may include medical therapy for complications and aneurysmectomy for intractable arrhythmias or heart failure unresponsive to medical and catheter-based therapy (89).

Pseudoaneurysm results from myocardial rupture that is contained by pericardium or scar tissue. The wall of a pseudoaneurysm has no endocardium or myocardium and is formed of parietal pericardium and thrombus. Pseudoaneurysm is more commonly seen in the inferior and inferolateral walls and less commonly in the anterior wall.

Unlike the mouth of a true aneurysm, the mouth of a pseudoaneurysm is smaller than the actual size of the aneurysmal segment (Fig 15), and the pseudoaneurysm is dyskinetic during both systole and diastole. Pseudoaneurysm is commonly associated with mural thrombosis, and typically there is pericardial enhancement at delayed-enhancement MR imaging. Pseudoaneurysm carries a high risk of expansion and rupture (30%–45%), so emergency surgery is a frequent necessity in this situation (88,89).

Pericardial Effusion or Pericarditis

Pericardial effusion is seen in 25% of patients with MI and is most common in those with cardiac failure, anterior-wall MI, and large infarcts. At MR imaging, simple fluid pericardial effusion typically is seen as low signal intensity on double inversion-recovery black-blood images and high signal intensity on SSFP images. Hemorrhagic effusion most commonly has high signal intensity with all

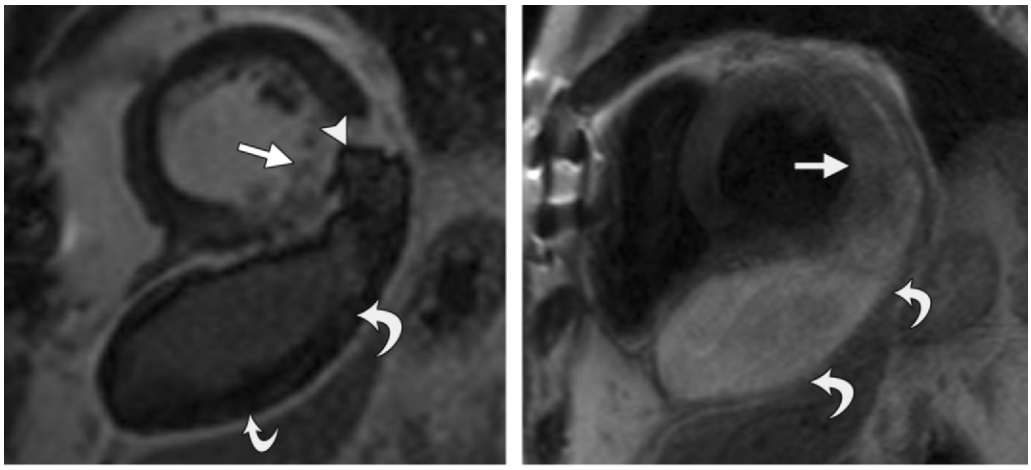

a. b.

Figure 16. Hemorrhagic pericardial effusion in a 47-year-old man. **(a)** Short-axis delayed-enhancement image shows a full-thickness transmural infarct (straight arrow) in the midinferolateral and inferior walls. There is a dark area of hemorrhagic microvascular obstruction (arrowhead) within this scar, which is continuous with a large collection in the pericardium (curved arrows) that has high signal intensity within it, consistent with a hemorrhagic pericardial effusion. **(b)** Short-axis T2-weighted black-blood image shows myocardial edema (straight arrow) and high-signal-intensity pericardial effusion (curved arrows).

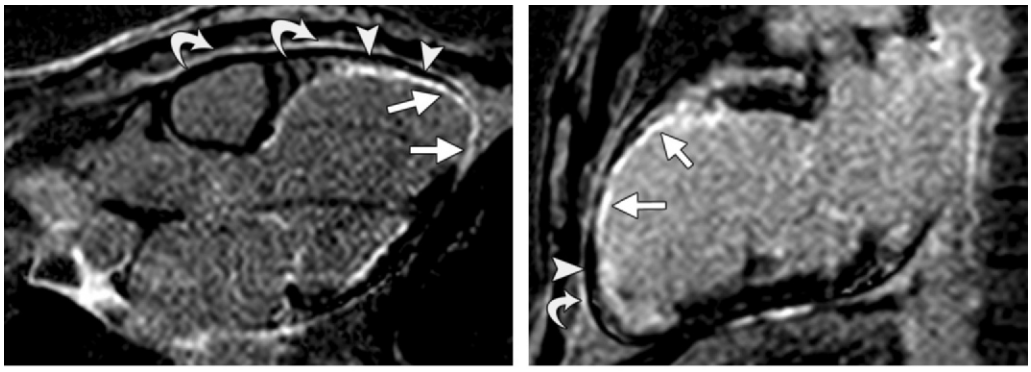

a. b.

Figure 17. Pericarditis in a 71-year-old man with MI. **(a)** Three-chamber delayed-enhancement image shows full-thickness scarring in the apex and lateral wall (straight arrows), consistent with transmural MI. In addition, there is also pericardial enhancement anterior to the RV (curved arrows), which is consistent with pericardial inflammation. There is a thin layer of dark pericardial effusion (arrowheads) between the infarct and inflamed pericardium. **(b)** Two-chamber delayed-enhancement image shows transmural and near-transmural scarring in the anterior wall and apex (straight arrows), consistent with MI. In addition, a thin layer of pericardial enhancement (curved arrow) is seen anterior to the LV, again consistent with pericardial inflammation. There is a thin layer of dark pericardial effusion (arrowhead) between the infarct and inflamed pericardium.

sequences, although this may vary depending on the age of the blood products (Fig 16).

Pericarditis (inflammation of the pericardium) is more commonly seen in patients with transmural acute MI, but the overall incidence is decreasing thanks to improved treatment times for acute MI. In early pericarditis, infarct-related myocardial inflammation spreads to the pericardium. Late pericarditis (Dressler syndrome), seen in 3%–4% of patients with MI, is typically an autoimmune reaction and has no particular temporal relationship with MI.

Black-blood, cine, and delayed-enhancement MR imaging are useful for evaluating the morphologic and functional aspects of pericardial diseases. In acute pericarditis, pericardial thickening and fluid can be seen on black-blood and delayed-enhancement images (Fig 17). If acute pericarditis progresses to a chronic inflammatory stage, pericardial thickening with or without fluid and delayed hyperenhancement can be seen.

Figure 18. Thrombus in a 63-year-old man. **(a)** Four-chamber phase-sensitive inversion-recovery delayed-enhancement image shows a small area of dark thrombus (curved arrow) adjacent to a scarred segment of apical myocardium (straight arrow). **(b)** On a short-axis delayed-enhancement image with a long inversion time (600 msec), the thrombus stays dark (curved arrow) while the normal myocardium has turned grayish (straight arrow). This feature allows thrombus to be distinguished from a cardiac mass (which is vascular and would also turn grayish, similar to the myocardium).

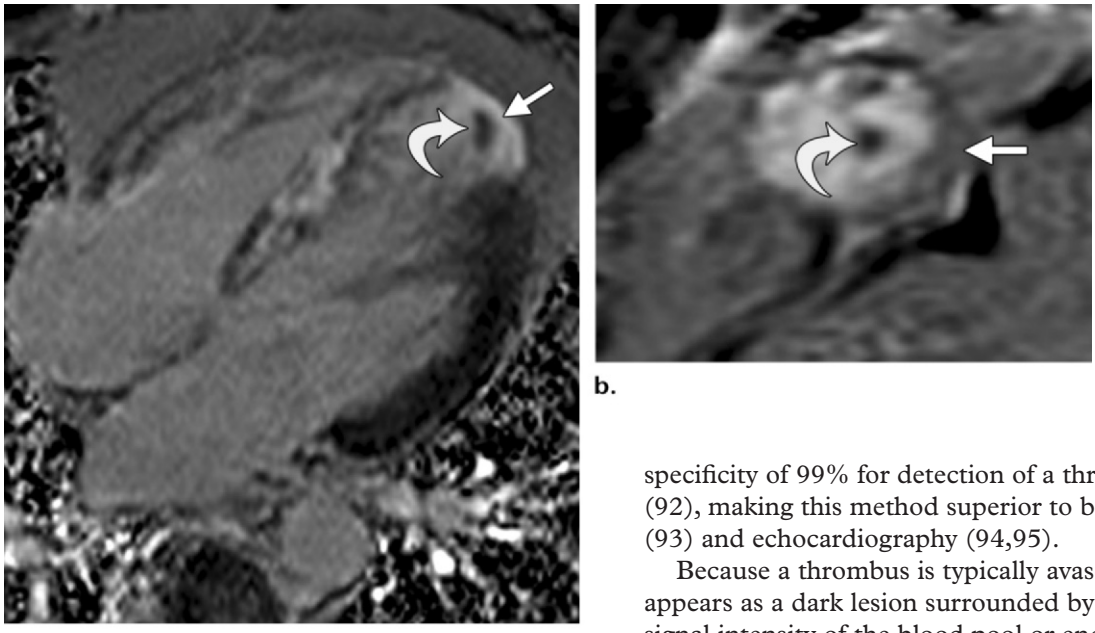

a. b.

If the condition further progresses to the chronic fibrotic stage, the pericardium will be thickened with fibrosis or calcification and without any delayed hyperenhancement (90). Features of pericardial constriction such as diastolic septal bounce, diastolic restraint, conical deformity of the ventricles, and exaggerated inspiratory septal bowing (ventricular interdependence) may also be seen on cine and black-blood images in the chronic fibrotic stage (27,28).

Thrombus

Thrombus occurs on the endocardial surfaces overlying the infarct secondary to endocardial inflammation during the acute phase of MI. Thrombus is seen in 20% of all infarcts, 40% of anterior infarcts, and 60% of apical infarcts (91). Patients with infarct are five times more likely to have a thrombus than patients without infarct who have similar levels of systolic dysfunction (21), demonstrating that scarring is a major risk factor for thrombus formation.

Although echocardiography is typically used to detect a thrombus, MR imaging offers higher contrast resolution, allowing detection of even small thrombi. Although a thrombus may be seen as an intermediate-signal-intensity mass on cine SSFP images, small thrombi may be difficult to detect with this technique. The delayed-enhancement technique has a sensitivity of 88% and specificity of 99% for detection of a thrombus (92), making this method superior to both SSFP (93) and echocardiography (94,95).

Because a thrombus is typically avascular, it appears as a dark lesion surrounded by the bright signal intensity of the blood pool or endocardial scar on delayed-enhancement images (Fig 18a). A thrombus can be distinguished from other cardiac masses through use of a delayed-enhancement image with a long inversion time (500–600 msec), which will cause the blood pool, myocardium, and most other masses to become grayish while the thrombus remains dark (Fig 18b). A chronic thrombus may be organized and have a degree of neovascularity, which will result in heterogeneous intermediate signal intensity and patchy areas of hyperenhancement (95).

Mitral Regurgitation

Mitral regurgitation is seen in 11%–59% of patients with MI and is a major independent adverse prognostic determinant; mitral regurgitation is associated with an increase in heart failure and mortality (96). The various factors associated with development of mitral regurgitation are global and regional remodeling; papillary muscle rupture, infarction (Fig 19a), or dysfunction; and acute systolic mitral annular dilatation. In the acute phase, mitral regurgitation can be caused by rupture of the papillary muscle or one of its heads; although rare, this occurrence is typically severe and can be fatal. Rupture is more common in the posteromedial papillary muscle group that is supplied by the posterior descending artery than in the anterolateral muscle group that is supplied by diagonal or marginal branches.

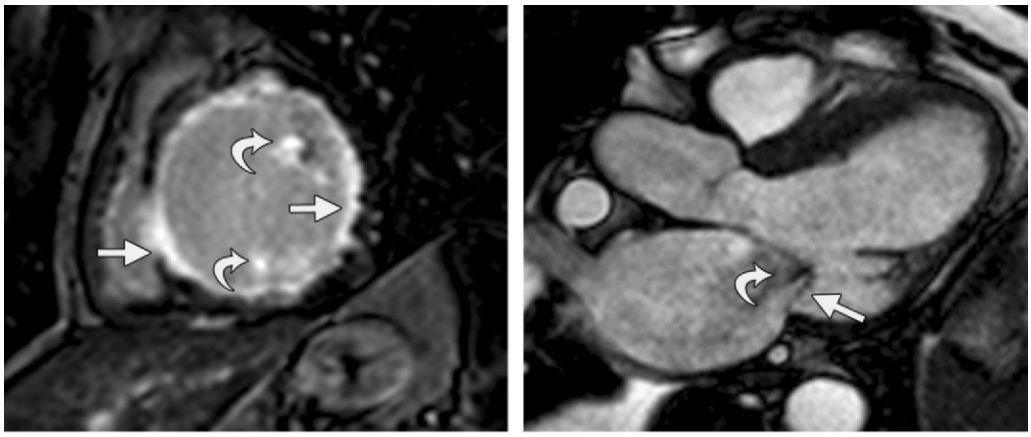

a. b.

Figure 19. Mitral regurgitation in MI. **(a)** Short-axis delayed-enhancement image in a 57-year-old man shows mostly subendocardial scarring and a focal spot of transmural scarring (straight arrows) in the LAD, LCX, and RCA territories. In addition, there is scarring in the anterolateral and posteromedial groups of papillary muscles (curved arrows), also consistent with papillary muscle infarction. **(b)** Three-chamber SSFP image in a 65-year-old man shows a tethered posterior mitral leaflet (straight arrow) due to geometric LV remodeling, resulting in a jet of mitral regurgitation (curved arrow).

Ischemic mitral regurgitation was previously attributed to ischemic papillary muscle dysfunction associated with dilatation and loss of contraction of the mitral annulus (Movie 2 [online]). However, the current thinking is that mitral regurgitation is caused by restricted leaflet motion that results in incomplete valve closure (Movie 3 [online]); local ischemic remodeling leads to apical and posterior papillary muscle displacement and wall-motion abnormalities that result in tethering of the posterior mitral valve leaflet (Fig 19b) and lead to systolic tenting and incomplete closure of the valve. This effect may be augmented by global remodeling that results in dilatation and loss of contraction of the mitral annulus (96).

Cine SSFP MR imaging allows identification and characterization of the mechanism of regurgitation, and the severity can be quantified with velocity-encoded phase-contrast sequences. The prognosis is worse in the setting of ischemic mitral regurgitation because of associated LV remodeling and systolic dysfunction. Unfortunately, ischemic mitral regurgitation has a high rate of recurrence, even after surgical repair of the mitral valve (96).

Infarction of RV and Right Atrium

RV infarction may occur as a complication of inferior-wall MI in up to 25% of patients (97). RV infarction may also be seen secondary to chronic lung disease or RV hypertrophy. Isolated RV infarcts require volume loading, unlike LV infarcts, which require reduction of afterload. Atrial infarction (most commonly in the right atrium) is seen in 10% of inferior wall infarcts and is detected with delayed-enhancement MR imaging (98).

Chronic Congestive Heart Failure

Chronic congestive heart failure can occur after MI from either a single large healed infarct or multiple small infarcts (discussed earlier). Associated mitral regurgitation worsens the cardiac failure by placing greater mechanical demand on an already-weakened LV myocardium. The combination of cine SSFP, velocity-encoded phase-contrast, and delayed-enhancement MR imaging allows comprehensive assessment of global and regional ventricular function, qualitative and quantitative mitral valve function, and the presence and extent of irreversible myocardial damage.

Emerging Clinical Applications of MR Imaging in MI

MR Imaging in Emergency Room

MR imaging has been used in the emergency setting for evaluation of patients presenting with acute chest pain. MR imaging can be used to rule out ACS, acute aortic dissection, acute pulmonary embolism, and acute myocarditis. Approximately 30% of patients with typical chest pain do not have ACS. When complementary pulse sequences are incorporated, MR imaging has sensitivity and specificity of 95% and 100%, respectively, for diagnosis of aortic dissection (99), 80% and 100%,

respectively, for diagnosis of acute pulmonary embolism (100), and 88% and 91%, respectively, for diagnosis of acute myocarditis (25).

ACS can be evaluated with cine, rest perfusion, and delayed-enhancement images. Kwong et al (34) found that MR imaging improved sensitivity and specificity for diagnosis of ACS to 84% and 85%, respectively, values superior to those achieved using ECG levels alone (80% and 61%, respectively) or enzyme levels alone (40% and 97%, respectively). The researchers used the presence of wall-motion abnormality and abnormal delayed hyperenhancement at MR imaging as diagnostic criteria for ACS; these were the strongest predictors of acute coronary events.

Cury et al (35) demonstrated that adding a T2-weighted sequence to this protocol improved the sensitivity (85% vs 84%), specificity (96% vs 85%), and accuracy (93% vs 84%) of MR imaging for diagnosis of ACS. In another study, edema on T2-weighted images could be seen in dogs as soon as 26 minutes after the onset of coronary occlusion; wall-motion abnormalities were also observed at a stage when delayed hyperenhancement was not seen (7).

After revascularization, segmental wall motion improves, but edema persists. In fact, edema can develop in the setting of myocardial damage before the presence of delayed hyperenhancement. The persistence of edema allows clinicians to assess the area at risk. Thus, MI can potentially be detected even before cardiac enzyme levels become elevated, which can occur up to 6 hours after the ischemic event.

Coronary Artery Imaging

The culprit lesion responsible for an acute MI is typically identified with invasive coronary angiography. CT angiography is increasingly used in evaluation of coronary artery disease and has a high negative predictive value. This method can act as a gatekeeper for patients who require invasive coronary angiography for diagnosis and interventional management. MR coronary angiography can be used to evaluate proximal coronary arteries. Although MR coronary angiography was initially performed by acquiring images in planes optimized for each coronary artery, this procedure is now performed with a simple axial acquisition of a 3D whole-heart T2-prepared SSFP sequence with ECG gating and respiratory gating (the latter using a navigator sequence to track diaphragmatic movements).

Targeted MR coronary angiography at 1.5 T has sensitivity of 50%–92% and specificity of 42% for detection of obstructive coronary artery disease (101), whereas whole-heart coronary MR angiography has sensitivity of 82% and specificity of 90% (102). Although MR imaging is an attractive option because it is noninvasive and does not require radiation, this procedure is not ideal for evaluation of distal segments. Improved image quality and shorter imaging time for the 3D whole-heart technique can be achieved with high-field-strength magnets, such as 3 T or 7 T, and 32-channel coils (103) have the potential to further increase diagnostic accuracy.

MR imaging of the coronary wall has also been attempted; selective attenuation of the lumen–blood pool signal makes this modality useful for serial noninvasive follow-up studies. Wall thickening and positive remodeling have been demonstrated in both symptomatic and asymptomatic patients before the development of luminal stenosis (104,105). In one study, a thicker wall was seen in diabetic patients with renal insufficiency than in those without (105). Atherosclerotic plaques can be detected with superparamagnetic iron oxide; plaques are identified by increased susceptibility defects on T1-weighted GRE images resulting from increased iron oxide uptake by macrophages in inflammatory plaques (106). Delayed enhancement of the coronary vessel wall after administration of gadolinium can provide information about endothelial leakage and fibrosis or inflammation (107).

MR Spectroscopy

MR spectroscopy is a technique that provides quantitative information on cardiac metabolism by determining the area under each spectral peak of nuclei such as phosphorus-31, hydrogen-1, and sodium-23 or by using a hyperpolarization technique with carbon-13–labeled molecules (108). ^{1}H and ^{31}P MR spectroscopy techniques have been used to evaluate ischemia and infarction (108).

Although a reduction of the phosphocreatinine (PCr)–adenosine triphosphate (ATP) ratio has been demonstrated in ischemic heart disease—a reduction that reverses with revascularization (109)—MR spectroscopy has not yet been established as a reliable modality for evaluating myocardial viability because of its limited spatial resolution relative to the size and heterogeneity of an infarct (108). However, with the advent of high-field-strength magnets, novel gating techniques, and 3D acquisition, MR spectroscopy may be used in the future to evaluate cardiac metabolism (108).

Evaluation of New Therapeutic Approaches

MR imaging can be used to evaluate novel therapeutic approaches to reducing reperfusion injury, infarct size, and area at risk and increasing salvaged area. In addition, MR imaging can be used to assess the effect of these approaches in modifying prognostic indicators such as adverse remodeling, arrhythmia risk, and device effectiveness. The size of the MI scar can also be a useful surrogate end point in clinical trials assessing drugs for the treatment of MI, including both early-screening studies and long-term trials (7); even if early benefit is not clear, a reduction in infarct size may alter ventricular remodeling and improve prognosis.

MR imaging has also been used to evaluate the efficacy of intracoronary stem cell therapy in MI. Initial animal studies demonstrated that within 8 days of bone marrow cells being transplanted in coronary arteries, newly formed myocardium occupied 68% of the infarcted portion of the LV (110). Although initial trials suggested that stem cells were more effective than traditional therapy (111), recent MR imaging studies have demonstrated no additional effect of stem cells on ventricular volumes, ejection fraction, or regional function (112,113). Further, the early beneficial effects demonstrated in the BOOST trial were no longer evident after 18 months (114).

Conclusion

MR imaging plays an important role in evaluation of various aspects of MI. This imaging modality is useful in establishing the diagnosis of MI in patients who present outside the diagnostic time frame of altered cardiac enzyme levels or with clinical features of acute MI but without an angiographic culprit lesion. MR imaging provides vital information on risk stratification, including data on scar burden, viability, and microvascular obstruction. MR imaging is also useful in detecting complications such as aneurysms, pericarditis, ventricular septal defect, thrombus, and mitral regurgitation. Finally, MR imaging is particularly useful in predicting response to therapy, while scar size demonstrated with delayed-enhancement MR imaging can serve as a useful surrogate end point in clinical trials.

Acknowledgment.— The authors wish to thank Megan Griffiths, scientific writer for the Imaging Institute, Cleveland Clinic, for her editorial assistance.

Disclosures of Conflicts of Interest.—**D.K.:** *Related financial activities:* career development award from the American College of Cardiology Foundation and GE Healthcare. *Other financial activities:* none. **S.D.F.:** *Related financial activities:* none. *Other financial activities:* consultant for Philips Healthcare.

References

1. Ryan TJ, Antman EM, Brooks NH, et al. 1999 update: ACC/AHA guidelines for the management of patients with acute myocardial infarction: a report of the American College of Cardiology/American Heart Association Task Force on Practice Guidelines (Committee on Management of Acute Myocardial Infarction). J Am Coll Cardiol 1999;34(3):890–911.
2. Thygesen K, Alpert JS, White HD; Joint ESC/ACCF/AHA/WHF Task Force for the Redefinition of Myocardial Infarction. Universal definition of myocardial infarction. J Am Coll Cardiol 2007;50(22):2173–2195.
3. Kim RJ, Fieno DS, Parrish TB, et al. Relationship of MRI delayed contrast enhancement to irreversible injury, infarct age, and contractile function. Circulation 1999;100(19):1992–2002.
4. Rehwald WG, Fieno DS, Chen EL, Kim RJ, Judd RM. Myocardial magnetic resonance imaging contrast agent concentrations after reversible and irreversible ischemic injury. Circulation 2002;105(2):224–229.
5. Schwitter J, Wacker CM, van Rossum AC, et al. MR-IMPACT: comparison of perfusion-cardiac magnetic resonance with single-photon emission computed tomography for the detection of coronary artery disease in a multicentre, multivendor, randomized trial. Eur Heart J 2008;29(4):480–489.
6. Kellman P, Arai AE. Imaging sequences for first pass perfusion: a review. J Cardiovasc Magn Reson 2007;9(3):525–537.
7. Abdel-Aty H, Zagrosek A, Schulz-Menger J, et al. Delayed enhancement and T2-weighted cardiovascular magnetic resonance imaging differentiate acute from chronic myocardial infarction. Circulation 2004;109(20):2411–2416.
8. Abdel-Aty H, Simonetti O, Friedrich MG. T2-weighted cardiovascular magnetic resonance imaging. J Magn Reson Imaging 2007;26(3):452–459.
9. Kellman P, Aletras AH, Mancini C, McVeigh ER, Arai AE. T2-prepared SSFP improves diagnostic confidence in edema imaging in acute myocardial infarction compared to turbo spin echo. Magn Reson Med 2007;57(5):891–897.
10. Aletras AH, Kellman P, Derbyshire JA, Arai AE. ACUT2E TSE-SSFP: a hybrid method for T2-weighted imaging of edema in the heart. Magn Reson Med 2008;59(2):229–235.
11. Huang TY, Liu YJ, Stemmer A, Poncelet BP. T2 measurement of the human myocardium using a T2-prepared transient-state TrueFISP sequence. Magn Reson Med 2007;57(5):960–966.
12. Giri S, Chung YC, Merchant A, et al. T2 quantification for improved detection of myocardial edema. J Cardiovasc Magn Reson 2009;11:56.
13. Hamdan A, Asbach P, Wellnhofer E, et al. A prospective study for comparison of MR and CT imaging for detection of coronary artery stenosis. JACC Cardiovasc Imaging 2011;4(1):50–61.

14. Bogaert J, Francone M. Cardiovascular magnetic resonance in pericardial diseases. J Cardiovasc Magn Reson 2009;11:14.
15. Simpson RM, Keegan J, Firmin DN. MR assessment of regional myocardial mechanics. J Magn Reson Imaging 2013;37(3):576–599.
16. Nagel E, Stuber M, Lakatos M, Scheidegger MB, Boesiger P, Hess OM. Cardiac rotation and relaxation after anterolateral myocardial infarction. Coron Artery Dis 2000;11(3):261–267.
17. Kramer CM, Lima JA, Reichek N, et al. Regional differences in function within noninfarcted myocardium during left ventricular remodeling. Circulation 1993;88(3):1279–1288.
18. Kim RJ, Albert TS, Wible JH, et al. Performance of delayed-enhancement magnetic resonance imaging with gadoversetamide contrast for the detection and assessment of myocardial infarction: an international, multicenter, double-blinded, randomized trial. Circulation 2008;117(5):629–637.
19. Ricciardi MJ, Wu E, Davidson CJ, et al. Visualization of discrete microinfarction after percutaneous coronary intervention associated with mild creatine kinase-MB elevation. Circulation 2001;103(23):2780–2783.
20. Wagner A, Mahrholdt H, Holly TA, et al. Contrast-enhanced MRI and routine single photon emission computed tomography (SPECT) perfusion imaging for detection of subendocardial myocardial infarcts: an imaging study. Lancet 2003;361(9355):374–379.
21. Kim HW, Farzaneh-Far A, Kim RJ. Cardiovascular magnetic resonance in patients with myocardial infarction: current and emerging applications. J Am Coll Cardiol 2009;55(1):1–16.
22. Larson DM, Menssen KM, Sharkey SW, et al. "False-positive" cardiac catheterization laboratory activation among patients with suspected ST-segment elevation myocardial infarction. JAMA 2007;298(23):2754–2760.
23. Wang K, Asinger RW, Marriott HJ. ST-segment elevation in conditions other than acute myocardial infarction. N Engl J Med 2003;349(22):2128–2135.
24. Assomull RG, Lyne JC, Keenan N, et al. The role of cardiovascular magnetic resonance in patients presenting with chest pain, raised troponin, and unobstructed coronary arteries. Eur Heart J 2007;28(10):1242–1249.
25. Friedrich MG, Sechtem U, Schulz-Menger J, et al. Cardiovascular magnetic resonance in myocarditis: a JACC White Paper. J Am Coll Cardiol 2009;53(17):1475–1487.
26. Pilgrim TM, Wyss TR. Takotsubo cardiomyopathy or transient left ventricular apical ballooning syndrome: a systematic review. Int J Cardiol 2008;124(3):283–292.
27. Taylor AM, Dymarkowski S, Verbeken EK, Bogaert J. Detection of pericardial inflammation with late-enhancement cardiac magnetic resonance imaging: initial results. Eur Radiol 2006;16(3):569–574.
28. Moon JC, McKenna WJ, McCrohon JA, Elliott PM, Smith GC, Pennell DJ. Toward clinical risk assessment in hypertrophic cardiomyopathy with gadolinium cardiovascular magnetic resonance. J Am Coll Cardiol 2003;41(9):1561–1567.
29. Patel MR, Cawley PJ, Heitner JF, et al. Detection of myocardial damage in patients with sarcoidosis. Circulation 2009;120(20):1969–1977.
30. Cheong BY, Muthupillai R, Nemeth M, et al. The utility of delayed-enhancement magnetic resonance imaging for identifying nonischemic myocardial fibrosis in asymptomatic patients with biopsy-proven systemic sarcoidosis. Sarcoidosis Vasc Diffuse Lung Dis 2009;26(1):39–46.
31. Litmanovich D, Bankier AA, Cantin L, Raptopoulos V, Boiselle PM. CT and MRI in diseases of the aorta. AJR Am J Roentgenol 2009;193(4):928–940.
32. Stein PD, Chenevert TL, Fowler SE, et al. Gadolinium-enhanced magnetic resonance angiography for pulmonary embolism: a multicenter prospective study (PIOPED III). Ann Intern Med 2010;152(7):434–443, W142–W143.
33. Tandri H, Saranathan M, Rodriguez ER, et al. Noninvasive detection of myocardial fibrosis in arrhythmogenic right ventricular cardiomyopathy using delayed-enhancement magnetic resonance imaging. J Am Coll Cardiol 2005;45(1):98–103.
34. Kwong RY, Schussheim AE, Rekhraj S, et al. Detecting acute coronary syndrome in the emergency department with cardiac magnetic resonance imaging. Circulation 2003;107(4):531–537.
35. Cury RC, Shash K, Nagurney JT, et al. Cardiac magnetic resonance with T2-weighted imaging improves detection of patients with acute coronary syndrome in the emergency department. Circulation 2008;118(8):837–844.
36. Gheorghiade M, Sopko G, De Luca L, et al. Navigating the crossroads of coronary artery disease and heart failure. Circulation 2006;114(11):1202–1213.
37. White JA, Patel MR. The role of cardiovascular MRI in heart failure and the cardiomyopathies. Cardiol Clin 2007;25(1):71–95, vi.
38. McCrohon JA, Moon JC, Prasad SK, et al. Differentiation of heart failure related to dilated cardiomyopathy and coronary artery disease using gadolinium-enhanced cardiovascular magnetic resonance. Circulation 2003;108(1):54–59.
39. Cummings KW, Bhalla S, Javidan-Nejad C, Bierhals AJ, Gutierrez FR, Woodard PK. A pattern-based approach to assessment of delayed enhancement in nonischemic cardiomyopathy at MR imaging. RadioGraphics 2009;29(1):89–103.
40. van Dockum WG, ten Cate FJ, ten Berg JM, et al. Myocardial infarction after percutaneous transluminal septal myocardial ablation in hypertrophic obstructive cardiomyopathy: evaluation by contrast-enhanced magnetic resonance imaging. J Am Coll Cardiol 2004;43(1):27–34.
41. Raff GL, O'Neill WW, Gentry RE, et al. Microvascular obstruction and myocardial function after acute myocardial infarction: assessment by using contrast-enhanced cine MR imaging. Radiology 2006;240(2):529–536.
42. Friedrich MG, Abdel-Aty H, Taylor A, Schulz-Menger J, Messroghli D, Dietz R. The salvaged area at risk in reperfused acute myocardial infarction as visualized by cardiovascular magnetic resonance. J Am Coll Cardiol 2008;51(16):1581–1587.

43. Aletras AH, Tilak GS, Natanzon A, et al. Retrospective determination of the area at risk for reperfused acute myocardial infarction with T2-weighted cardiac magnetic resonance imaging: histopathological and displacement encoding with stimulated echoes (DENSE) functional validations. Circulation 2006;113(15):1865–1870.
44. Eitel I, Desch S, Fuernau G, et al. Prognostic significance and determinants of myocardial salvage assessed by cardiovascular magnetic resonance in acute reperfused myocardial infarction. J Am Coll Cardiol 2010;55(22):2470–2479.
45. Croisille P, Kim HW, Kim RJ. Controversies in cardiovascular MR imaging: T2-weighted imaging should not be used to delineate the area at risk in ischemic myocardial injury. Radiology 2012;265(1): 12–22.
46. Kim RJ, Wu E, Rafael A, et al. The use of contrast-enhanced magnetic resonance imaging to identify reversible myocardial dysfunction. N Engl J Med 2000;343(20):1445–1453.
47. Choi KM, Kim RJ, Gubernikoff G, Vargas JD, Parker M, Judd RM. Transmural extent of acute myocardial infarction predicts long-term improvement in contractile function. Circulation 2001;104 (10):1101–1107.
48. Rogers WJ Jr, Kramer CM, Geskin G, et al. Early contrast-enhanced MRI predicts late functional recovery after reperfused myocardial infarction. Circulation 1999;99(6):744–750.
49. Wu KC, Zerhouni EA, Judd RM, et al. Prognostic significance of microvascular obstruction by magnetic resonance imaging in patients with acute myocardial infarction. Circulation 1998;97(8):765–772.
50. Nijveldt R, Hofman MB, Hirsch A, et al. Assessment of microvascular obstruction and prediction of short-term remodeling after acute myocardial infarction: cardiac MR imaging study. Radiology 2009;250(2):363–370.
51. Beek AM, Kühl HP, Bondarenko O, et al. Delayed contrast-enhanced magnetic resonance imaging for the prediction of regional functional improvement after acute myocardial infarction. J Am Coll Cardiol 2003;42(5):895–901.
52. Wu E, Ortiz JT, Tejedor P, et al. Infarct size by contrast enhanced cardiac magnetic resonance is a stronger predictor of outcomes than left ventricular ejection fraction or end-systolic volume index: prospective cohort study. Heart 2008;94(6):730–736.
53. Orn S, Manhenke C, Anand IS, et al. Effect of left ventricular scar size, location, and transmurality on left ventricular remodeling with healed myocardial infarction. Am J Cardiol 2007;99(8):1109–1114.
54. Kaandorp TA, Lamb HJ, Viergever EP, et al. Scar tissue on contrast-enhanced MRI predicts left ventricular remodelling after acute infarction. Heart 2007;93(3):375–376.
55. Bello D, Fieno DS, Kim RJ, et al. Infarct morphology identifies patients with substrate for sustained ventricular tachycardia. J Am Coll Cardiol 2005; 45(7):1104–1108.
56. Schmidt A, Azevedo CF, Cheng A, et al. Infarct tissue heterogeneity by magnetic resonance imaging identifies enhanced cardiac arrhythmia susceptibility in patients with left ventricular dysfunction. Circulation 2007;115(15):2006–2014.
57. Kwon DH, Halley CM, Carrigan TP, et al. Extent of left ventricular scar predicts outcomes in ischemic cardiomyopathy patients with significantly reduced systolic function: a delayed hyperenhancement cardiac magnetic resonance study. JACC Cardiovasc Imaging 2009;2(1):34–44.
58. Cheong BY, Muthupillai R, Wilson JM, et al. Prognostic significance of delayed-enhancement magnetic resonance imaging: survival of 857 patients with and without left ventricular dysfunction. Circulation 2009;120(21):2069–2076.
59. Roes SD, Kelle S, Kaandorp TA, et al. Comparison of myocardial infarct size assessed with contrast-enhanced magnetic resonance imaging and left ventricular function and volumes to predict mortality in patients with healed myocardial infarction. Am J Cardiol 2007;100(6):930–936.
60. Mahrholdt H, Wagner A, Parker M, et al. Relationship of contractile function to transmural extent of infarction in patients with chronic coronary artery disease. J Am Coll Cardiol 2003;42(3):505–512.
61. Reimer KA, Jennings RB. The "wavefront phenomenon" of myocardial ischemic cell death. II. Transmural progression of necrosis within the framework of ischemic bed size (myocardium at risk) and collateral flow. Lab Invest 1979;40(6):633–644.
62. Fieno DS, Kim RJ, Chen EL, Lomasney JW, Klocke FJ, Judd RM. Contrast-enhanced magnetic resonance imaging of myocardium at risk: distinction between reversible and irreversible injury throughout infarct healing. J Am Coll Cardiol 2000;36(6):1985–1991.
63. Cerqueira MD, Weissman NJ, Dilsizian V, et al. Standardized myocardial segmentation and nomenclature for tomographic imaging of the heart: a statement for healthcare professionals from the Cardiac Imaging Committee of the Council on Clinical Cardiology of the American Heart Association. Circulation 2002;105(4):539–542.
64. Bondarenko O, Beek AM, Hofman MB, et al. Standardizing the definition of hyperenhancement in the quantitative assessment of infarct size and myocardial viability using delayed contrast-enhanced CMR. J Cardiovasc Magn Reson 2005;7 (2):481–485.
65. Amado LC, Gerber BL, Gupta SN, et al. Accurate and objective infarct sizing by contrast-enhanced magnetic resonance imaging in a canine myocardial infarction model. J Am Coll Cardiol 2004;44(12): 2383–2389.
66. Heiberg E, Ugander M, Engblom H, et al. Automated quantification of myocardial infarction from MR images by accounting for partial volume effects: animal, phantom, and human study. Radiology 2008;246(2):581–588.
67. Hsu LY, Ingkanisorn WP, Kellman P, Aletras AH, Arai AE. Quantitative myocardial infarction on delayed enhancement MRI. Part II: Clinical application of an automated feature analysis and combined thresholding infarct sizing algorithm. J Magn Reson Imaging 2006;23(3):309–314.

68. Kannel WB, Abbott RD. Incidence and prognosis of unrecognized myocardial infarction: an update on the Framingham study. N Engl J Med 1984;311 (18):1144–1147.
69. Kwong RY, Chan AK, Brown KA, et al. Impact of unrecognized myocardial scar detected by cardiac magnetic resonance imaging on event-free survival in patients presenting with signs or symptoms of coronary artery disease. Circulation 2006;113(23): 2733–2743.
70. Barbier CE, Bjerner T, Johansson L, Lind L, Ahlström H. Myocardial scars more frequent than expected: magnetic resonance imaging detects potential risk group. J Am Coll Cardiol 2006;48(4):765–771.
71. Beek AM, Nijveldt R, van Rossum AC. Intramyocardial hemorrhage and microvascular obstruction after primary percutaneous coronary intervention. Int J Cardiovasc Imaging 2010;26(1):49–55.
72. Ganame J, Messalli G, Dymarkowski S, et al. Impact of myocardial haemorrhage on left ventricular function and remodelling in patients with reperfused acute myocardial infarction. Eur Heart J 2009;30 (12):1440–1449.
73. Greenwood JP, Maredia N, Younger JF, et al. Cardiovascular magnetic resonance and single-photon emission computed tomography for diagnosis of coronary heart disease (CE-MARC): a prospective trial. Lancet 2012;379(9814):453–460. 74. Tsukiji M, Nguyen P, Narayan G, et al. Peri-infarct ischemia determined by cardiovascular magnetic resonance evaluation of myocardial viability and stress perfusion predicts future cardiovascular events in patients with severe ischemic cardiomyopathy. J Cardiovasc Magn Reson 2006;8(6):773–779.
75. Neizel M, Korosoglou G, Lossnitzer D, et al. Impact of systolic and diastolic deformation indexes assessed by strain-encoded imaging to predict persistent severe myocardial dysfunction in patients after acute myocardial infarction at follow-up. J Am Coll Cardiol 2010;56(13):1056–1062.
76. Bax JJ, Poldermans D, Elhendy A, Boersma E, Rahimtoola SH. Sensitivity, specificity, and predictive accuracies of various noninvasive techniques for detecting hibernating myocardium. Curr Probl Cardiol 2001;26(2):147–186.
77. Baer FM, Voth E, Schneider CA, Theissen P, Schicha H, Sechtem U. Comparison of low-dose dobutamine-gradient-echo magnetic resonance imaging and positron emission tomography with [18F] fluorodeoxyglucose in patients with chronic coronary artery disease: a functional and morphological approach to the detection of residual myocardial viability. Circulation 1995;91(4):1006–1015.
78. Kühl HP, Beek AM, van der Weerdt AP, et al. Myocardial viability in chronic ischemic heart disease: comparison of contrast-enhanced magnetic resonance imaging with (18)F-fluorodeoxyglucose positron emission tomography. J Am Coll Cardiol 2003;41(8):1341–1348.
79. Bauer RW, Kerl JM, Fischer N, et al. Dual-energy CT for the assessment of chronic myocardial infarction in patients with chronic coronary artery disease: comparison with 3-T MRI. AJR Am J Roentgenol 2010;195(3):639–646.
80. Bax JJ, Wijns W, Cornel JH, Visser FC, Boersma E, Fioretti PM. Accuracy of currently available techniques for prediction of functional recovery after revascularization in patients with left ventricular dysfunction due to chronic coronary artery disease: comparison of pooled data. J Am Coll Cardiol 1997; 30(6):1451–1460.
81. Lardo AC, Cordeiro MA, Silva C, et al. Contrast-enhanced multidetector computed tomography viability imaging after myocardial infarction: characterization of myocyte death, microvascular obstruction, and chronic scar. Circulation 2006;113(3):394–404.
82. Buckley O, Di Carli M. Predicting benefit from revascularization in patients with ischemic heart failure: imaging of myocardial ischemia and viability. Circulation 2011;123(4):444–450.
83. Hamilton-Craig C, Seltmann M, Ropers D, Achenbach S. Myocardial viability by dual-energy delayed enhancement computed tomography. JACC Cardiovasc Imaging 2011;4(2):207–208.
84. Bleeker GB, Kaandorp TA, Lamb HJ, et al. Effect of posterolateral scar tissue on clinical and echocardiographic improvement after cardiac resynchronization therapy. Circulation 2006;113(7):969–976.
85. Figueras J, Cortadellas J, Soler-Soler J. Left ventricular free wall rupture: clinical presentation and management. Heart 2000;83(5):499–504.
86. Tikiz H, Balbay Y, Atak R, Terzi T, Genç Y, Kütük E. The effect of thrombolytic therapy on left ventricular aneurysm formation in acute myocardial infarction: relationship to successful reperfusion and vessel patency. Clin Cardiol 2001;24(10):656–662.
87. Glower DG, Lowe EL. Left ventricular aneurysm. In: Edmunds LH, ed. Cardiac surgery in the adult. New York, NY: McGraw-Hill, 1997; 677.
88. Konen E, Merchant N, Gutierrez C, et al. True versus false left ventricular aneurysm: differentiation with MR imaging—initial experience. Radiology 2005;236(1):65–70.
89. Heatlie GJ, Mohiaddin R. Left ventricular aneurysm: comprehensive assessment of morphology, structure and thrombus using cardiovascular magnetic resonance. Clin Radiol 2005;60(6):687–692.
90. Zurick AO, Bolen MA, Kwon DH, et al. Pericardial delayed hyperenhancement with CMR imaging in patients with constrictive pericarditis undergoing surgical pericardiectomy: a case series with histopathological correlation. JACC Cardiovasc Imaging 2011;4(11):1180–1191.
91. Fuster V, Halperin JL. Left ventricular thrombi and cerebral embolism. N Engl J Med 1989;320(6): 392–394.
92. Srichai MB, Junor C, Rodriguez LL, et al. Clinical, imaging, and pathological characteristics of left ventricular thrombus: a comparison of contrast-enhanced magnetic resonance imaging, transthoracic echocardiography, and transesophageal echocardiography with surgical or pathological validation. Am Heart J 2006;152(1):75–84.

93. Weinsaft JW, Kim HW, Shah DJ, et al. Detection of left ventricular thrombus by delayed-enhancement cardiovascular magnetic resonance: prevalence and markers in patients with systolic dysfunction. J Am Coll Cardiol 2008;52(2):148–157.
94. Mollet NR, Dymarkowski S, Volders W, et al. Visualization of ventricular thrombi with contrast-enhanced magnetic resonance imaging in patients with ischemic heart disease. Circulation 2002;106(23):2873–2876.
95. Keeley EC, Hillis LD. Left ventricular mural thrombus after acute myocardial infarction. Clin Cardiol 1996;19(2):83–86.
96. Bursi F, Enriquez-Sarano M, Jacobsen SJ, Roger VL. Mitral regurgitation after myocardial infarction: a review. Am J Med 2006;119(2):103–112.
97. Kumar A, Abdel-Aty H, Kriedemann I, et al. Contrast-enhanced cardiovascular magnetic resonance imaging of right ventricular infarction. J Am Coll Cardiol 2006;48(10):1969–1976.
98. Lazar EJ, Goldberger J, Peled H, Sherman M, Frishman WH. Atrial infarction: diagnosis and management. Am Heart J 1988;116(4):1058–1063.
99. Clough RE, Schaeffter T, Taylor PR. Magnetic resonance imaging for aortic dissection. Eur J Vasc Endovasc Surg 2010;39(4):514; author reply 514–515.
100. Kluge A, Luboldt W, Bachmann G. Acute pulmonary embolism to the subsegmental level: diagnostic accuracy of three MRI techniques compared with 16-MDCT. AJR Am J Roentgenol 2006;187(1):W7–W14.
101. Kim WY, Danias PG, Stuber M, et al. Coronary magnetic resonance angiography for the detection of coronary stenoses. N Engl J Med 2001;345(26):1863–1869.
102. Sakuma H, Ichikawa Y, Chino S, Hirano T, Makino K, Takeda K. Detection of coronary artery stenosis with whole-heart coronary magnetic resonance angiography. J Am Coll Cardiol 2006;48(10):1946–1950.
103. Liu X, Bi X, Huang J, Jerecic R, Carr J, Li D. Contrast-enhanced whole-heart coronary magnetic resonance angiography at 3.0 T: comparison with steady-state free precession technique at 1.5 T. Invest Radiol 2008;43(9):663–668.
104. Kim WY, Stuber M, Börnert P, Kissinger KV, Manning WJ, Botnar RM. Three-dimensional black-blood cardiac magnetic resonance coronary vessel wall imaging detects positive arterial remodeling in patients with nonsignificant coronary artery disease. Circulation 2002;106(3):296–299.
105. Kim WY, Astrup AS, Stuber M, et al. Subclinical coronary and aortic atherosclerosis detected by magnetic resonance imaging in type 1 diabetes with and without diabetic nephropathy. Circulation 2007;115(2):228–235.
106. Korosoglou G, Weiss RG, Kedziorek DA, et al. Noninvasive detection of macrophage-rich atherosclerotic plaque in hyperlipidemic rabbits using "positive contrast" magnetic resonance imaging. J Am Coll Cardiol 2008;52(6):483–491.
107. Ibrahim T, Makowski MR, Jankauskas A, et al. Serial contrast-enhanced cardiac magnetic resonance imaging demonstrates regression of hyperenhancement within the coronary artery wall in patients after acute myocardial infarction. JACC Cardiovasc Imaging 2009;2(5):580–588.
108. Holloway C, Clarke K. Is MR spectroscopy of the heart ready for humans? Heart Lung Circ 2010;19(3):154–160.
109. Weiss RG, Bottomley PA, Hardy CJ, Gerstenblith G. Regional myocardial metabolism of high-energy phosphates during isometric exercise in patients with coronary artery disease. N Engl J Med 1990;323(23):1593–1600.
110. Orlic D, Kajstura J, Chimenti S, et al. Bone marrow cells regenerate infarcted myocardium. Nature 2001;410(6829):701–705.
111. Hirsch A, Nijveldt R, van der Vleuten PA, et al. Intracoronary infusion of autologous mononuclear bone marrow cells in patients with acute myocardial infarction treated with primary PCI: pilot study of the multicenter HEBE trial. Catheter Cardiovasc Interv 2008;71(3):273–281.
112. Tendera M, Wojakowski W, Ruzyllo W, et al. REGENT Investigators. Intracoronary infusion of bone marrow-derived selected CD34+CXCR4+ cells and non-selected mononuclear cells in patients with acute STEMI and reduced left ventricular ejection fraction: results of randomized, multicentre Myocardial Regeneration by Intracoronary Infusion of Selected Population of Stem Cells in Acute Myocardial Infarction (REGENT) trial. Eur Heart J 2008;30(11):1313–1321.
113. Janssens S, Dubois C, Bogaert J, et al. Autologous bone marrow-derived stem-cell transfer in patients with ST-segment elevation myocardial infarction: double-blind, randomised controlled trial. Lancet 2006;367(9505):113–121.
114. Meyer GP, Wollert KC, Lotz J, et al. Intracoronary bone marrow cell transfer after myocardial infarction: eighteen months' follow-up data from the randomized, controlled BOOST (BOne marrOw transfer to enhance ST-elevation infarct regeneration) trial. Circulation 2006;113(10):1287–1294.

MR Imaging of Myocardial Infarction

Prabhakar Rajiah, MD, FRCR • Milind Y. Desai, MD • Deborah Kwon, MD • Scott D. Flamm, MD, MBA

RadioGraphics 2013; 33:1383–1412 • **Published online** 10.1148/rg.335125722 • **Content Codes:** CA MR

Page 1387
Delayed-enhancement imaging is the most important technique for evaluation of MI. It is the most accurate method for diagnosing MI or nonischemic cardiomyopathies, quantifying the scar, assessing viability, and evaluating thrombus.

Page 1390
The delayed-enhancement technique has high sensitivity for identification of both acute (99%) and chronic (94%) MI, with the ability to detect as little as 1 gram of irreversibly damaged tissue.

Page 1391
However, the clinical presentation of acute MI is variable and occasionally overlaps with that of other conditions that cause myocardial injury; in these cases, MR imaging can be useful for accurate diagnosis.

Page 1393
A large subset of patients presenting with congestive cardiac failure are diagnosed with dilated or nondilated cardiomyopathy based on echocardiography results; coronary artery disease accounts for 62% of congestive cardiac failure cases.

Page 1398
Silent MI is associated with a six- to 11-fold increased risk of major cardiac events and a worse prognosis.